GROUND-STATE PROPERTIES OF ULTRA-COLD ATOMIC GASES

A THESIS
SUBMITTED TO THE DEPARTMENT OF PHYSICS
AND THE INSTITUTE OF ENGINEERING AND SCIENCE
OF BILKENT UNIVERSITY
IN PARTIAL FULFILLMENT OF THE REQUIREMENTS
FOR THE DEGREE OF
DOCTOR OF PHILOSOPHY

By
Sevilay Sevinçli
September 2008

I certify that I have read this thesis and that in my opinion it is fully adequate, in scope and in quality, as a dissertation for the degree of doctor of philosophy.

Prof. Bilal Tanatar (Supervisor)

I certify that I have read this thesis and that in my opinion it is fully adequate, in scope and in quality, as a dissertation for the degree of doctor of philosophy.

Assist. Prof. Mehmet Özgür Oktel

I certify that I have read this thesis and that in my opinion it is fully adequate, in scope and in quality, as a dissertation for the degree of doctor of philosophy.

Assist. Prof. Ceyhun Bulutay

I certify that I have read this thesis and that in my opinion it is fully adequate, in scope and in quality, as a dissertation for the degree of doctor of philosophy.

Assoc. Prof. Hakkı Turgay Kaptanoğlu

I certify that I have read this thesis and that in my opinion it is fully adequate, in scope and in quality, as a dissertation for the degree of doctor of philosophy.

Assoc. Prof. Valeriu Moldoveanu

Approved for the Institute of Engineering and Science:

Prof. Mehmet Baray,
Director of Institute of Engineering and Science

Abstract

GROUND-STATE PROPERTIES OF ULTRA-COLD ATOMIC GASES

Sevilay Sevinçli
PhD in Physics
Supervisor: Prof. Bilal Tanatar
September 2008

After the observation of Bose-Einstein condensation, the developments in the experimental control and measurement methods provided the realization of basic models of many-body physics using dilute, ultra-cold gases. This thesis presents a theoretical study on a number of topics on ultra-cold atomic gas systems. First, a simple model of trapped, degenerate ultra-cold plasma is presented. Using the variational approach, the dependence of the cloud size on electron density is studied, electron and ion densities are also calculated by means of modified Thomas-Fermi model. Next, the behavior of a single particle hopping on a three dimensional cubic optical lattice in the presence of a Mott insulator of bosons is investigated. Localization problem of a single fermion is studied and effects of lattice anisotropy, and higher impurity bands are also calculated. Then, a two-dimensional condensate with long-range, attractive gravity-like interaction is studied. Ground-state properties, dynamics, and vortex states are analyzed by using a variational approach for this system. Finally, the thermodynamics of the harmonically trapped ideal gas obeying generalized exclusion statistics is investigated.

Keywords: ultra-cold plasma, ideal g-on gases, optical lattices, Bose-Fermi mixtures, gravity-like interaction

Özet

ULTRA-SOĞUK ATOMİK GAZLARIN TABAN-DURUMU ÖZELLİKLERİ

Sevilay Sevinçli
Fizik Doktora
Tez Yöneticisi: Prof. Bilal Tanatar
Eylül 2008

Bose-Einstein yoğuşmasının deneysel olarak gözlemlenmesinden sonra, ultra-soğuk gazlarda deneysel kontrol ve ölçüm metotlarındaki ilerlemeler çok parçacık fiziğinin temel modellerinin hayata geçirilmesini sağladı. Bu tezde, ultra-soğuk atomik gaz sistemleriyle ilgili teorik çalışmalar yapılmıştır. İlk olarak, tuzaklanmış, dejenere ultra-soğuk plazma sistemi için varyasyonel metot kullanılarak, plazma bulutunun genişliğinin elektron yoğunluğuna bağımlılığı çalışıldı. Modifiye Thomas-Fermi metodu kullanılarak elektron ve iyon yoğunlukları hesaplandı. İkinci olarak, üç boyutlu kübik optik örgüde, bozonlar Mott yalıtkanı durumundayken tek bir fermiyon için lokalizasyon problemi araştırıldı. Daha sonra, uzak-erimli kütleçekimi benzeri etkileşime sahip iki boyutlu Bose-Einstein yoğuşuğunun taban durumu özellikleri, dinamiği ve girdap durumları varyasyonel metotla analiz edildi. Son olarak, harmonik olarak tuzaklanmış ve genelleştirilmiş dışarlama istatistiğine uyan ideal gazın termodinamik özellikleri araştırıldı.

Anahtar sözcükler: ultra-soğuk plazma, ideal g-on gazları, optik örgüler, Bose-Fermi karışımları, kütleçekimi benzeri etkileşim

Acknowledgement

First of all I would like to thank to my thesis supervisor Prof. Bilal Tanatar for his guidance. I should also express my appreciation to Assist. Prof. M. Özgür Oktel for valuable discussions.

I should express my thanks to the faculty members and the staff of the Department of Physics for the scientific environment.

I thank to my coauthors; R. Onur Umucalılar and Ahmet Keleş.

I am gratefull to my friends for cheerful memories. I would like to thank to A. Levent Subaşı for our furious discussions on physics and life, and Selcen Aytekin for her friendship and support.

I am thankfull to my family for their constant support.

Finally, I am gratefull to my husband Haldun, to whom this thesis dedicated, for his encouragement throughout my studies and for his endless patience and love.

Contents

List of Figures

List of Tables

Chapter 1

Introduction

After the experimental realization of Bose-Einstein condensation (BEC) in 1995 [1, 2], the study of degenerate quantum gases has grown explosively and researchers from different areas of physics (atomic physics, quantum optics, condensed matter physics, etc.) have been working together.

The Bose-Einstein condensation was predicted by Einstein [3], on the basis of the statistical description of the quanta of light by S. N. Bose [4], in 1925. A large fraction of the bosonic atoms condense to the state of lowest energy as a consequence of quantum statistical effects, when a gas is cooled below a critical temperature. In other words, the wavepackets overlap when atoms are cooled to the point where the de Broglie wavelength, $\lambda_{dB} = (2\pi\hbar^2/mk_BT)^{1/2}$, is comparable to the interatomic separation, and there is a quantum mechanical phase transition which is called Bose-Einstein condensation.

The experimental observation of BEC, and hence dilute, ultra-cold gases provides a realization of the basic models of many-body physics. Over the last years various experimental and theoretical studies on these systems are being performed, such as collective excitations and rotational properties of the condensates, quantized vortices and vortex lattice, interference and coherence phenomena, two component condensates and boson-fermion mixtures, and spinor condensates [5, 6]. By the help of sympathetic cooling, Fermi degeneracy has also been achieved [7].

Two major experimental developments in dilute ultra-cold gases make it possible to investigate strongly correlated systems. First is the ability to tune the interaction strength (i.e. the s-wave scattering length a) by Feshbach resonances [8, 9], and second is the ability to generate strong periodic potentials for ultra-cold atoms through optical lattices [10]. Jaksch *et al.* [11] proposed that quantum phase transition from a superfluid to a Mott-insulator state would be realized in a system of BEC in optical lattices by raising the lattice depth. Greiner *et al.* [10] observed this superfluid-Mott-insulator transition by loading the condensate into an optical lattice. Another new direction in the study of degenerate quantum gases is the condensate with long-range interactions. There is a proposal for the occurrence of gravity-like $1/r$ interactions [12], and BEC in gases with dipole-dipole interaction was realized experimentally [13]. The total control and tunability of the interactions in quantum degenerate systems make it possible to study some basic problems in many-body physics, and especially to investigate new regimes that have never been accessible in condensed matter or nuclear physics.

Parallel to the recent experimental advances, we study a number of quantum gaseous systems, such as ultra-cold plasmas, ideal gases obeying fractional statistics, Bose-Fermi mixtures in optical lattice, and condensates with long-range $1/r$ interaction in this thesis. Ultra-cold degenerate gases are studied within the mean-field theory generally, and in the following sections of this chapter, the basic formalism to study these systems is given. The theory is expressed by a non-linear differential equation, Gross-Pitaevskii equation, for the order parameter that is described classically.

1.1 The Gross-Pitaevskii Equation

In second quantization picture, the many-body Hamiltonian for the system of N interacting bosons with trapping potential V_{ext} is given by [14]

$$\begin{aligned} \hat{H} &= \int d\mathbf{r}\, \hat{\Psi}^\dagger(\mathbf{r}) \left[\frac{\hbar^2}{2m}\nabla^2 + V_{ext}(\mathbf{r}) \right] \hat{\Psi}(\mathbf{r}) \\ &+ \frac{1}{2}\int d\mathbf{r}\, d\mathbf{r}'\, \hat{\Psi}^\dagger(\mathbf{r})\hat{\Psi}^\dagger(\mathbf{r}')V(\mathbf{r}-\mathbf{r}')\hat{\Psi}(\mathbf{r}')\hat{\Psi}(\mathbf{r}), \end{aligned} \tag{1.1}$$

where $\hat{\Psi}(\mathbf{r})$ and $\hat{\Psi}^\dagger(\mathbf{r})$ are the boson field operators annihilating and creating a particle at position $\mathbf{r}$, respectively, and $V(\mathbf{r}-\mathbf{r}')$ is the two-body interatomic potential.

To overcome the problem of solving full many-body Hamiltonian, mean-field theories are developed for interacting systems. Bogoliubov [15] formulated the basic idea of a mean-field description for a dilute Bose gas. Separation of the condensate contribution from the bosonic field operator is the key point of this formalism. The field operator generally can be written as sum of a product of the single-particle wave functions $\Psi_\alpha(\mathbf{r})$ and the corresponding annihilation operator a_α

$$\hat{\Psi}(\mathbf{r}) = \sum_\alpha \Psi_\alpha(\mathbf{r}) a_\alpha, \tag{1.2}$$

where the bosonic creation and annihilation operators $a_\alpha^\dagger$ and a_α are defined as

$$a_\alpha^\dagger |n_0, n_1, ..., n_\alpha, ...\rangle = \sqrt{n_\alpha + 1}\,|n_0, n_1, ..., n_\alpha + 1, ...\rangle, \tag{1.3}$$

$$a_\alpha |n_0, n_1, ..., n_\alpha, ...\rangle = \sqrt{n_\alpha}\,|n_0, n_1, ..., n_\alpha - 1, ...\rangle, \tag{1.4}$$

where n_α are the eigenvalues of the number operator $\hat{n}_\alpha = a_\alpha^\dagger a_\alpha$ of atoms in the single-particle α-state. These operators obey the general commutation rules:

$$[a_\alpha, a_\beta^\dagger] = \delta_{\alpha\beta}, \quad [a_\alpha, a_\beta] = 0, \quad [a_\alpha^\dagger, a_\beta^\dagger] = 0. \tag{1.5}$$

Condensation occurs when the number of atoms n_0 of a particular single particle state becomes very large, i.e. $n_0 \equiv N_0 \gg 1$ and the ratio N_0/N is finite in the thermodynamic limit $N \to \infty$. States with N_0 and $N_0 + 1 \approx N_0$ correspond to the same physical configuration, in this limit. Then, the bosonic operators can be treated like numbers, $a_0 = a_0^\dagger = \sqrt{N_0}$. The single-particle state

$\Psi_0 = 1/\sqrt{V}$ having zero momentum corresponds to condensed state for a uniform gas in volume V. Consequently, $\Psi(\mathbf{r})$ can be decomposed in the form

$$\hat{\Psi}(\mathbf{r}) = \sqrt{N_0/V} + \Psi'(\mathbf{r}), \tag{1.6}$$

where $\Psi'(\mathbf{r})$ is the depletion of the condensate. Thus, the generalization of the Bogoliubov formalism in the case of nonuniform and time-dependent configuration is given by

$$\hat{\Psi}(\mathbf{r},t) = \Phi(\mathbf{r},t) + \Psi'(\mathbf{r},t), \tag{1.7}$$

where $\Phi(\mathbf{r},t)$ is complex function which is defined as the expectation value of the field operator, $\Phi(\mathbf{r},t) \equiv \langle\hat{\Psi}(\mathbf{r},t)\rangle$, and the condensate density is its modulus: $\rho_0(\mathbf{r},t) = |\Phi(\mathbf{r},t)|^2$. This function is often called the wave function of the condensate.

If depletion is small, decomposition of the field operator in Equation 1.6 can be used. Time evolution of the field operator is obtained by Heisenberg equations with the many-body Hamiltonian, Equation 1.1,

$$\begin{aligned} i\hbar\frac{\partial}{\partial t}\hat{\Psi}(\mathbf{r},t) &= [\hat{\Psi},\hat{H}], \\ &= \left[-\frac{\hbar^2\nabla^2}{2m} + V_{ext} + \int d\mathbf{r}'\hat{\Psi}^\dagger(\mathbf{r}',t)V(\mathbf{r}',\mathbf{r})\hat{\Psi}(\mathbf{r}',t)\right]\hat{\Psi}(\mathbf{r},t). \end{aligned} \tag{1.8}$$

The two-body interaction potential can be replaced with an effective interaction $V(\mathbf{r}',\mathbf{r}) = g\delta(\mathbf{r}',\mathbf{r})$, since only binary collisions, which are characterized by the s-wave scattering length at low energy, are relevant, in the case of dilute and cold gas. The coupling constant g is related to the scattering length a through $g = 4\pi\hbar^2 a/m$. The scattering length can be positive or negative and this corresponds to an effective repulsion or attraction between the atoms, respectively. Then the field operator in Equation 1.8 is replaced with the order parameter Φ, and we obtain the equation

$$i\hbar\frac{\partial}{\partial t}\Phi(\mathbf{r},t) = \left[-\frac{\hbar^2\nabla^2}{2m} + V_{ext}(\mathbf{r}) + g|\Phi(\mathbf{r},t)|^2\right]\Phi(\mathbf{r},t), \tag{1.9}$$

which is called the time-dependent Gross-Pitaevskii equation (GPE), and derived independently by Gross [16] and Pitaevskii [17]. This equation is valid for the

case when s-wave scattering length is much smaller than the average distance between the atoms and that the number of the atoms in the condensate is much larger than one.

Time-dependent GPE may also be derived from the minimum action principle

$$\delta \int L dt = 0, \tag{1.10}$$

where the Lagrangian L is given by

$$L = \int d\mathbf{r} \frac{i\hbar}{2} \left(\Phi^* \frac{\partial \Phi}{\partial t} - \Phi \frac{\partial \Phi^*}{\partial t} \right) - E, \tag{1.11}$$

where E is the energy functional which is given by

$$E[\Phi] = \int d\mathbf{r} \left[\frac{\hbar^2}{2m} |\nabla \Phi|^2 + V_{ext}(\mathbf{r}) |\Phi|^2 + \frac{g}{2} |\nabla \Phi|^4 \right], \tag{1.12}$$

where the first term is the kinetic energy E_{kin}, the second one is the harmonic oscillator energy E_{ho}, and the last term is the mean-field interaction energy E_{int}. Diluteness of the gas is controlled by the dimensionless parameter $\bar{\rho}|a|^3$, the number of particles in a scattering volume, where $\bar{\rho}$ is the average density of the gas. If this parameter is much smaller than 1, the system is dilute or weakly interacting. However, to see the interaction effects, one should compare the interaction energy with the kinetic energy of the atoms in the trap. For the ground-state of the harmonic oscillator, the interaction energy can be written as $E_{int} \propto N^2|a|/a_{ho}^3$, where the average density is of the order of N/a_{ho}^3 and $a_{ho} = (\hbar/m\omega_{ho})^{1/2}$ is the harmonic oscillator length, and ω_{ho} is the trap frequency. Kinetic energy is of the order of $N\hbar\omega_{ho}$, thus $E_{kin} \propto N a_{ho}^{-2}$. Ratio of these two energies gives

$$\frac{E_{int}}{E_{kin}} \propto \frac{N|a|}{a_{ho}}, \tag{1.13}$$

which shows that even the very dilute gases can also exhibit an important non-ideal behavior.

The above formalism is valid only for the case that all the particles are in the condensate, that is in the zero temperature limit, since we assume that the condensate depletion $\hat{\Psi}' = 0$.

1.1.1 The Ground-state Solution

Within the mean-field theory, one can write the condensate wave function as $\Phi(\mathbf{r},t) = \phi(\mathbf{r})\mathrm{e}^{-\mathrm{i}\mu t/\hbar}$, where μ is the chemical potential. ϕ is real, and normalized to the total number of particles, $\int d\mathbf{r}\,\phi^2(\mathbf{r}) = N_0 = N$. Then the Gross-Pitaevskii equation 1.9, becomes

$$\left[-\frac{\hbar^2}{2m}\nabla^2 + V_{ext}(\mathbf{r}) + g\phi^2(\mathbf{r})\right]\phi(\mathbf{r}) = \mu\phi(\mathbf{r}), \tag{1.14}$$

time-independent GPE. This equation has the form of a nonlinear Schrödinger equation, and reduces to the usual one when there is no interaction. This equation can also be obtained by minimizing $E - \mu N$, where the chemical potential μ is the Lagrange multiplier which fixes the number of particles.

The solution of the Equation 1.14 minimizes the energy functional for a fixed number of particles. The energy is a function of density only for the ground-state, and can be written as

$$\begin{aligned} E[\rho] &= \int d\mathbf{r}\left[\frac{\hbar^2}{2m}|\nabla\sqrt{\rho}|^2 + \rho V_{ext}(\mathbf{r}) + \frac{g\rho^2}{2}\right], \\ &= E_{kin} + E_{ho} + E_{int}. \end{aligned} \tag{1.15}$$

The first term is usually called as quantum pressure, and one can easily see that it vanishes for the uniform systems. The balance between the quantum pressure and the interaction energy determines the healing or coherence length that is the length over which the gas heals from internal collisions.

We use the above formalism to describe various physical properties of the ultra-cold atomic gas systems at zero temperature.

The organization of this thesis is as follows. In Chapter 2, a simple model of quantum degenerate ultra-cold plasma which is trapped is presented. The dependence of the cloud size on electron density is studied variationally, and ion and electron densities are calculated by using modified Thomas-Fermi model. Then, localization problem of a fermionic particle on a boson Mott insulator background is investigated in Chapter 3. The effects of lattice anisotropy and higher impurity bands are calculated. Next, a two dimensional condensate with

attractive $1/r$ interaction is studied in Chapter 4. Ground-state properties, dynamics, and vortex states are analyzed by using a variational approach. Then, the thermodynamics of the ideal gas which obeys generalized exclusion statistics and is harmonically trapped in D dimensions is investigated in Chapter 5. Finally, concluding remarks are given in Chapter 6.

Chapter 2

Trapped Degenerate Ultra-cold Plasma

As a consequence of rapid developments in cooling and trapping mechanisms, number of experiments on ultra-cold systems increase and new directions are opened one after another. One of these new directions is the creation of an ultra-cold plasma. A plasma is a collection of free electrically charged particles, namely, the positively charged ions and the negatively charged electrons. A conventional neutral plasma is created by ionizing collisions between atoms and molecules. Most neutral plasmas such as the surface of the sun have temperatures on the order of thousands of Kelvin or more, since ionization usually results from energetic collisions between particles. Ultra-cold neutral plasmas give the opportunity to investigate a new regime in the field of plasma physics. Killian *et al.* [18] created an ultra-cold plasma by photoionization of atoms in a magneto-optical trap using a pulsed laser. They trapped the xenon atoms in a magneto-optical trap (MOT), and then photoionizing them. They obtained a plasma density of $2 \times 10^9 cm^{-3}$ with ion temperature 10 μK and electron temperature $100m$K. The size of the atom cloud was 200 μm while the Debye length could be as small as 500 nm. The initial observation was made with Xe atoms, but since then ultra-cold plasmas have been realized with Sr [19], Ca [20], Rb [21], and Cs [22] atoms.

Debye screening length λ_D is the length scale which is a measure to distinguish between the individual particle behavior and the collective behavior. It is the distance over which an electric field is screened by redistribution of electrons in the plasma, and is given by

$$\lambda_D = \sqrt{\frac{\epsilon_0 k_B T}{e^2 n}} \tag{2.1}$$

where ϵ_0 is the electric permittivity of vacuum, k_B is the Boltzmann constant, n is the electron density and e is the elementary charge. If the Debye length is larger than the size of the system an ionized gas is not a plasma.

A lot of interesting phenomena have been observed in ultra-cold plasmas, such as expansion of the plasma and recombination to form Rydberg atoms, both of which occur on the time scale of tens of microseconds. Initial temperature of the atomic cloud can be made very small, for example, Rydberg atom and ultra-cold plasma formations from a Bose Einstein Condensate has been demonstrated [23]. After the creation of an ultra-cold plasma the evolution of cold Rydberg atoms into a plasma was observed [19, 22, 24–34]. Cold dense samples of Rydberg atoms are fascinating since they combine atomic physics, plasma physics, and solid state physics.

In an ultra-cold plasma, the system is not in equilibrium and the ions and electrons have different kinetic energies. The ions and electrons thermalize among themselves, however since the plasma is not trapped so far, they do not thermalize with each other within the time scale of the experiment. Dynamical properties of the system can be investigated by understanding the thermalization of the plasma.

Such a novel nonequilibrium plasma allows for the possibility of both species being strongly coupled. A plasma becomes strongly coupled when the electrical interaction energy between the charged particles is higher than the thermal energy. The electron Coulomb coupling parameter, $\Gamma \approx e^2 n^{1/3}/k_B T$, is a measure of how strongly coupled the plasma is. For an ultra-cold plasma, this parameter is generally on the order of unity [19, 24–30]. In strongly coupled regime, recombination, collective modes, and thermalization are interesting properties

to investigate. However, it is still a challenge to reach this regime experimentally. One idea would be trapping the ions which would trap the electrons and form a stable system.

Ultra-cold neutral plasmas are ideal for experimental studies since they are highly controllable. It is possible to set the initial density and energy of the system by varying laser intensities and wavelengths. Optical absorption imaging and spectroscopy offer many new possibilities to examine these systems [35].

The electron pressure inside the plasma causes rapid expansion of the cloud, limiting the observation time to hundreds of microseconds and complicating the investigation of the properties of the ultra-cold plasma. Although the dynamical properties have yielded interesting phenomena, creation of a stable ultra-cold plasma will be interesting both theoretically and experimentally. Two types of traps could be used to stabilize ultra-cold plasma, an ion trap, such as Penning trap [36, 37] or the optical traps used in cold atom experiments [38, 39]. Recently, strongly magnetized and quasineutral ultra-cold plasma has been confined over several milliseconds in a nested Penning trap [40].

In this chapter, we study a simple model of quantum degenerate plasma. We assume that a quadratic trap for the ions has been set up and the cloud has been stabilized. We investigate the dependence of the cloud size on electron density by using a Gaussian variational wave function [41]. We assume that there is a constant density of electrons in the cloud giving rise to screened ion-ion interactions [42]. Then, we assume that all the electrons escape from the trap and leave a charged Bose gas and once again calculate the size of the cloud. Finally, for the same system, we study the case that density of electrons is not assumed to be a constant but used as a dynamical variable [43]. We calculate the densities of ions and electrons using a modified Thomas-Fermi model [44]. This method enables us to calculate the ion and electron densities separately, and as a result we find that the equilibrium structure is a neutral plasma. Thus the perfect screening property of the plasma is valid for even an ultra-cold degenerate system.

2.1 Creation of Ultra-cold Plasma

To create an ultra-cold neutral plasma, one should start with laser-cooled and trapped neutral atoms. Alkali atoms, alkaline-earth atoms, and metastable noble gas atoms are the most suitable atoms for these experiments, since they posses electric-dipole allowed transitions at convenient laser wavelengths. In an magneto-optical trap (MOT) as shown in Figure 2.1, up to 10^9 atoms can be cooled to millikelvin to microkelvin temperatures, and the density can be as high as $10^{11}\,\mathrm{cm}^{-3}$. Photons from properly arranged laser beams scatter off the atoms to generate the forces for cooling and trapping. The typical density distribution of atoms has a spherical Gaussian shape,

$$n_a(r) = n_0 \exp(-\mathrm{r}^2/2\sigma^2), \tag{2.2}$$

where $\sigma = 200 - 1500\,\mu$m is the width of the cloud [45]. These parameters can be adjusted by turning off the trap and allowing the cloud to expand.

First an atomic beam is slowed down with Zeeman slower (Figure 2.1), a beam of light counter propagating the atoms, which is red detuned, from the ${}^1S_0 - {}^1P_1$ atomic transition at 460.9 nm [35]. After slowing the atoms to velocity of about 50 cm/s, atoms are trapped and cooled to mK temperatures by using the six counter-propagating laser beams, also red detuned, along with a properly oriented magnetic field.

To form the plasma, the MOT magnets are turned off and atoms are ionized with photons from the cooling laser and from a pulsed dye laser whose wavelength is tuned just above the ionization continuum. After exciting the atoms to the ${}^1P_1$ level, atoms are photoionized by laser with wavelength ~ 412 nm. Figure 2.2 shows the atomic and ionic energy levels of Sr atoms with decay rates.

After photoionization, electrons carry the most of the energy since they are very light, and ions stay almost as cold as the initial atoms. Then, the electron cloud expands because of the kinetic energy they have, while the ions are immobile. The ions form a trap for electrons by means of Coulomb attraction which is produced by an internal electric field that is caused by charge imbalance. After the outer shell of electrons escape, the plasma is no longer neutral, however,

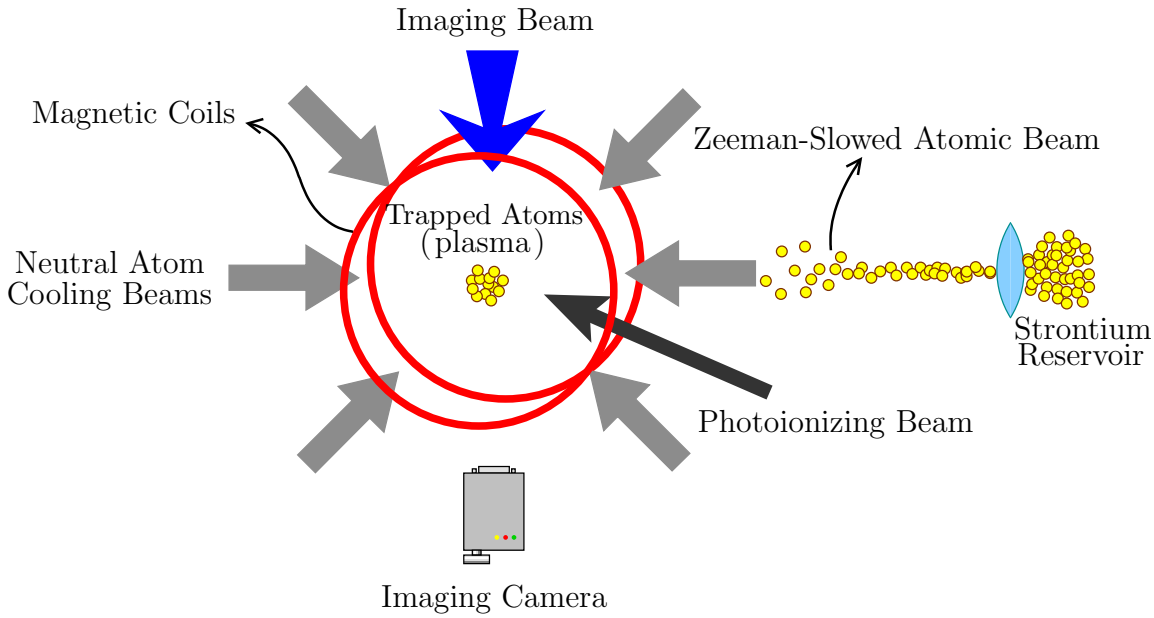

Figure 2.1: Experimental set-up for strontium plasma experiment. The MOT consists of a pair of anti-Helmholtz magnetic coils and 6 laser-cooling beams. After cooling, atoms are ionized and then, the imaging beam passes through the plasma and falls on a CCD camera. Adapted from [45].

the center of the cloud can be assumed as a neutral plasma [19, 24–30]. The density profiles of ions and electrons have a Gaussian shape like the original neutral atom cloud.

To obtain an absorption image of the plasma, a collimated laser beam, tuned near resonance with the $^2S_{1/2} - ^2P_{1/2}$ transition in the ions at 422 nm (Figure 2.2) is used [35]. Then, the imaging beam falls on an image intensified charge coupled device (CCD) camera at an adjustable delay time (t_{delay}) after photoionization. A shadow caused by scattering of photons by the ions is recorded by an intensified CCD camera. $^2P_{1/2}$ ions decay to the $^2D_{3/2}$ state 7% of the time, but this does not complicate the experiment because ions typically scatter less than one photon during the time the imaging beam is on [35].

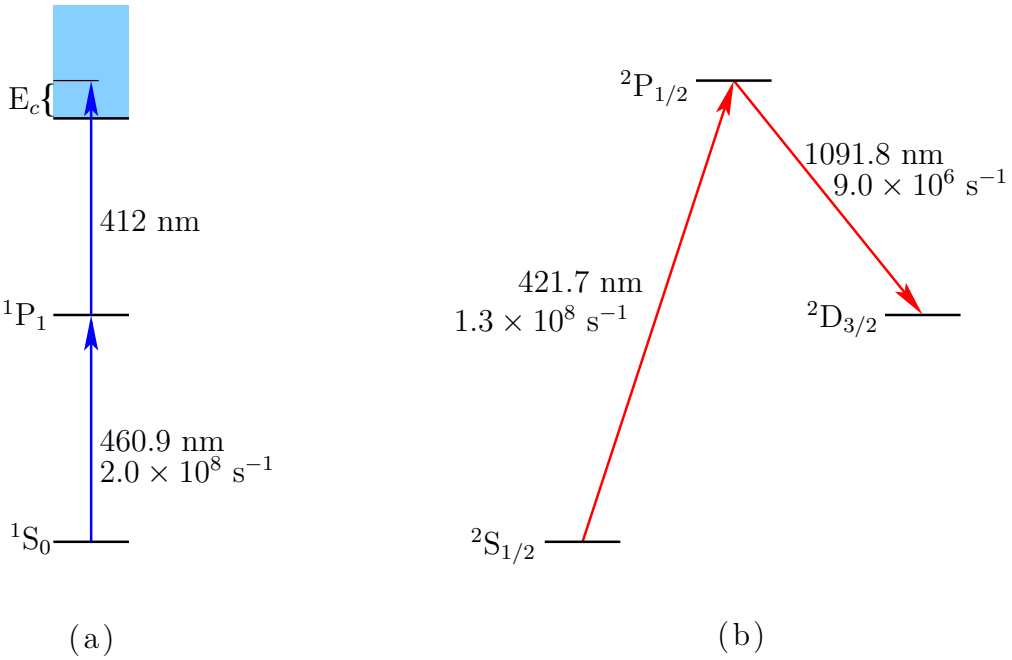

Figure 2.2: Strontium atomic and ionic levels with decay rates. (a) Neutral atoms are laser cooled and trapped in MOT operating on the ${}^1S_0 - {}^1P_1$ transition. E_c is the continuum energy. (b) Ions are imaged using the ${}^2S_{1/2} - {}^2P_{1/2}$ transition. Adapted from [45].

2.2 Degenerate Ultra-cold Plasma with Constant Electron Density

We describe the ion cloud as a Bose condensed system within the mean-field approximation. The ground state energy at zero temperature is given by the Gross-Pitaevskii energy functional

$$E = \int d\mathbf{r_1} \left\{ \frac{\hbar^2}{2m} |\nabla\psi(\mathbf{r_1})|^2 + \frac{1}{2} m\omega^2 r_1^2 |\psi(\mathbf{r_1})|^2 + \int d\mathbf{r_2}\, |\psi(\mathbf{r_1})|^2 |\psi(\mathbf{r_2})|^2\, U(\mathbf{r_1} - \mathbf{r_2}) \right\}, \tag{2.3}$$

where $U(\mathbf{r}) = (Z^2 e^2) \mathrm{e}^{-\mu \mathbf{r}}/\mathbf{r}$ is the Yukawa potential between the ions which are assumed to be in an isotropic harmonic oscillator potential $m\omega^2 \mathbf{r}^2/2$.

$U(\mathbf{r})$ models the screened Coulomb interaction between the ions through the screening parameter μ. $\psi(\mathbf{r})$ is the ion condensate wave function. We introduce dimensionless units by making the following transformation: (i) $\mathbf{r} \to l\mathbf{r}$, where $l = \sqrt{\hbar/m\omega}$ is oscillator length, and (ii) the energy is measured in units of $\hbar\omega$. Using the dimensionless quantities, we can rewrite the energy functional as

$$\frac{E}{\hbar\omega} = \frac{1}{2}\int d\mathbf{r_1}\left\{|\nabla\psi(\mathbf{r_1})|^2 + r_1^2|\psi(\mathbf{r_1})|^2\right\} + \gamma\int\int d\mathbf{r_1}d\mathbf{r_2}\frac{|\psi(\mathbf{r_1})|^2|\psi(\mathbf{r_2})|^2 e^{-\mu|\mathbf{r_1}-\mathbf{r_2}|}}{|\mathbf{r_1}-\mathbf{r_2}|}, \tag{2.4}$$

where

$$\gamma = \frac{(Z^2e^2)}{\hbar}\sqrt{\frac{m}{\hbar\omega}}, \tag{2.5}$$

is a dimensionless coupling strength for the interaction between the ions. It measures the ratio of interaction energy between the ions to their trapping energy. One should note that this parameter is totally different from the usual Coulomb coupling parameter which is used in plasma physics.

We use the variational principle to obtain the condensate wavefunction that minimizes the Gross-Pitaevskii functional. For simplicity, we choose a Gaussian trial wave function,

$$\psi(r) = \left[N\left(\frac{2\alpha}{\pi}\right)^{3/2}\right]^{1/2} e^{-\alpha r^2}, \tag{2.6}$$

with a variational parameter α. Note that ψ is normalized to N. The kinetic and external potential energy terms in the energy functional are easily calculated to be $3N\alpha/2$ and $3N/8\alpha$, respectively. To calculate the interaction term we go to the center-of-mass coordinate system,

$$\mathbf{R} = \frac{\mathbf{r_1}+\mathbf{r_2}}{2} \quad \text{and} \quad \mathbf{r} = \mathbf{r_1}-\mathbf{r_2}\,, \tag{2.7}$$

$$\mathbf{r_1} = \mathbf{R}+\frac{1}{2}\mathbf{r} \quad \text{and} \quad \mathbf{r_2} = \mathbf{R}-\frac{1}{2}\mathbf{r}\,. \tag{2.8}$$

By introducing this coordinate system, the interaction energy term becomes

$$E_I = \gamma N^2\left(\frac{2\alpha}{\pi}\right)^3\int\int d\mathbf{R}\,d\mathbf{r}\,\frac{\mathrm{e}^{-4\alpha\mathrm{R}^2}\mathrm{e}^{-(\alpha r^2+\mu r)}}{r}\,, \tag{2.9}$$

$$= \frac{2\gamma N^2}{\sqrt{\pi}}\alpha^{1/2} - \gamma N^2\mu\, e^{\frac{\mu^2}{4\alpha}}\,\mathrm{erfc}\left(\frac{\mu}{2\sqrt{\alpha}}\right)\,.$$

Finally, the total energy reads

$$\frac{E}{N\hbar\omega} = \frac{3}{2}\alpha + \frac{3}{8\alpha} + \frac{2N\gamma}{\sqrt{\pi}}\alpha^{1/2} - \gamma N\mu\, e^{\frac{\mu^2}{4\alpha}}\,\mathrm{erfc}\left(\frac{\mu}{2\sqrt{\alpha}}\right). \tag{2.10}$$

Minimizing the total energy with respect to α, we get

$$\frac{3}{2} - \frac{3}{8}\alpha^{-2} + \frac{N\gamma}{\sqrt{\pi}}\alpha^{-1/2} - \frac{N\gamma\mu^2}{2\sqrt{\pi}}\alpha^{-3/2} + \frac{N\gamma\mu^3}{4}\, e^{\frac{\mu^2}{4\alpha}}\,\mathrm{erfc}\left(\frac{\mu}{2\sqrt{\alpha}}\right)\alpha^{-2} = 0\,. \tag{2.11}$$

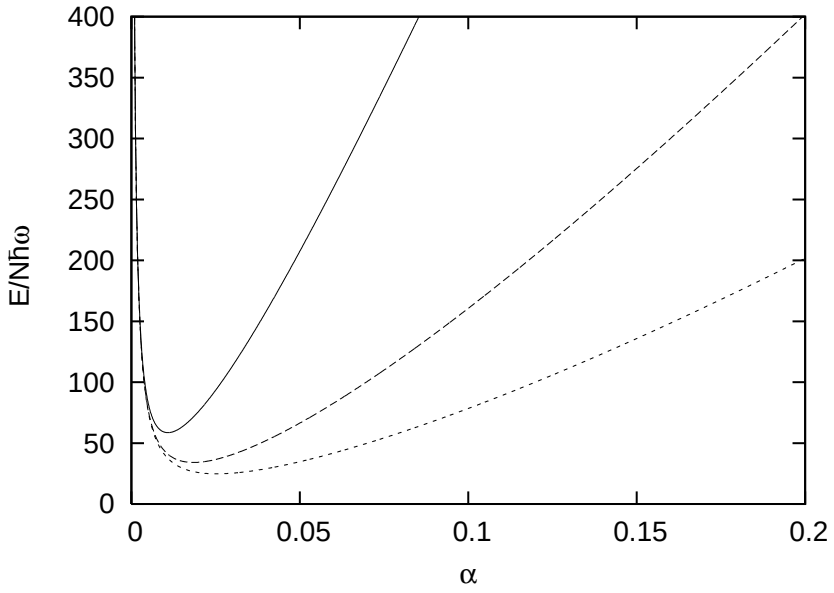

Figure 2.3: Total energy per particle in units of $\hbar\omega$ as a function of the variational parameter α for $N = 10^4$ atoms and different screening parameters for the Yukawa potential. Solid, dashed, and dotted lines are for $\mu = 1$, 2, and 3, respectively. The Coulomb coupling parameter is $\gamma = 1$.

Although the Coulomb coupling parameter γ is considered to be of the order of unity in the literature [46] for the charged Bose gas, realistic calculations of γ with experimental parameters [47] give a value of the order of 10^8. As an illustration we first give the variational parameter α dependence of the total energy per particle in units of $\hbar\omega$ for $\gamma = 1$ and $N = 10^4$ atoms in Figure 2.3. One can observe the minimum of the energy for various screening parameters in the figure. We shall address the more realistic case of large values of γ shortly.

The screening parameter μ in the screened Coulomb potential can be defined in terms of the density n_0 within the Thomas-Fermi (TF) approximation. The TF approximation assumes that a local internal chemical potential can be defined as a function of the electron concentration at that point. In the TF theory, the electron density is represented locally as a free particle system and the chemical potential is independent of position. Then, Thomas-Fermi screening length $1/\mu$ is defined as

$$\mu^2 = 4\left(\frac{3}{\pi}\right)^{1/3}\frac{n_0^{1/3}}{a_B}\,, \tag{2.12}$$

where a_B is the Bohr radius. The density at the center can be defined by means of the variational parameter α

$$n_0 = \frac{N}{\frac{4\pi}{3}\alpha^{-3/2}}\,. \tag{2.13}$$

Then, one can write the screening parameter as a function of the variational parameter α

$$\mu = \beta N^{1/6}\alpha^{1/4}\,, \tag{2.14}$$

where we have introduced a dimensionless quantity $\beta = (12/\pi)^{1/3}(l/a_B)^{1/2}$. Using the TF value of μ in Equation 2.10, the total energy per particle in terms of variational parameter α becomes

$$\frac{E}{N\hbar\omega} = \frac{3}{2}\alpha + \frac{3}{8\alpha} + \frac{2N\gamma}{\sqrt{\pi}}\alpha^{1/2} - \gamma N^{7/6}\beta\, e^{\frac{\beta^2 N^{1/3}}{4\alpha^{1/2}}}\,\mathrm{erfc}\left(\frac{\beta N^{1/6}}{2\alpha^{1/4}}\right)\alpha^{1/4}\,. \tag{2.15}$$

Minimizing the energy with respect to α, we obtain the relation

$$\begin{aligned}\frac{3}{2} - \frac{3}{8}\alpha^{-2} + \frac{N\gamma}{\sqrt{\pi}}\alpha^{-1/2} - \frac{N^{4/3}\gamma\beta^2}{4\sqrt{\pi}\alpha} \;&-\; \frac{N^{7/6}\gamma\beta}{4\alpha^{3/4}}\, e^{\frac{\beta^2 N^{1/3}}{4\alpha^{1/2}}}\,\mathrm{erfc}\left(\frac{\beta N^{1/6}}{2\alpha^{1/4}}\right) \\ &+\; \frac{N^{3/2}\gamma\beta^3}{8\alpha^{5/4}}\, e^{\frac{\beta^2 N^{1/3}}{4\alpha^{1/2}}}\,\mathrm{erfc}\left(\frac{\beta N^{1/6}}{2\alpha^{1/4}}\right) = 0\,.\end{aligned} \tag{2.16}$$

Figure 2.4 shows the dependence of the total energy per particle in units of $\hbar\omega$ on α, which is the inverse square of the cloud size, for $N = 10^4$ and the Coulomb coupling parameter $\gamma = 10^8$. It can be seen that there is still a minimum of energy for the realistic parameters. We solve Equation 2.16 numerically and find

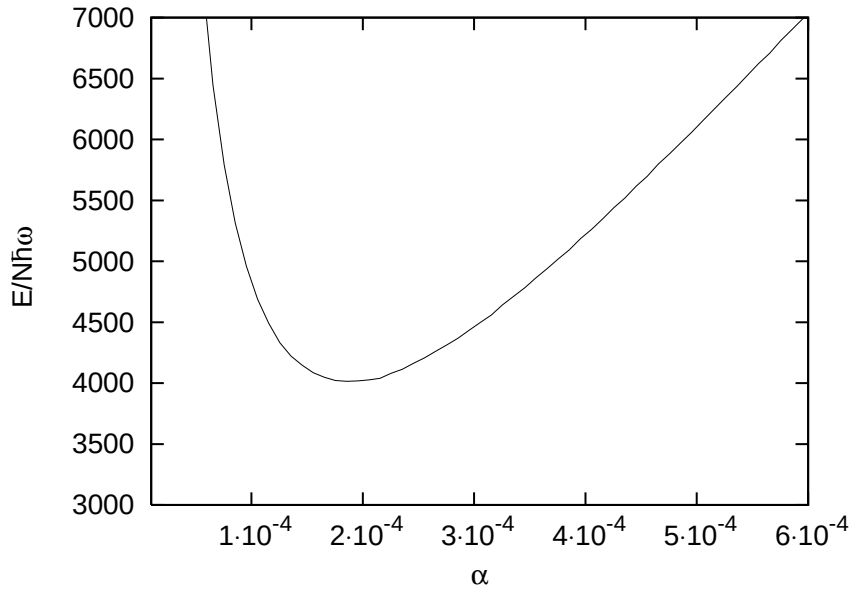

Figure 2.4: Total energy per particle in units of $\hbar\omega$ as a function of the variational parameter α for $N = 10^4$ atoms for Yukawa potential. The Coulomb coupling parameter is $\gamma = 10^8$.

the variational parameter α for various values of the parameters N, μ and γ. Our estimate of the cloud size relies on the experimental parameters of Chen *et al.* [47] who had $N = 10^4$ atoms. Thus, for 10^4 atoms we obtain the cloud size for the screened Coulomb interaction to be $\sim 15\,\mu$m for which the trap frequency is approximately 10^4 Hz. In Figure 2.5, the dependence of the size of a Bose condensed ionic cloud on the electron density which is obtained using the Thomas-Fermi screening picture is shown. Two limiting behaviors are evident. For the large values of the screening parameter μ, the cloud size, $1/\sqrt{\alpha}$, decreases as expected, since the screening reduces the range of the Coulomb potential. As the screening parameter μ goes to zero the value of the cloud size corresponds to that of bare Coulomb potential case, i.e. charged Bose gas.

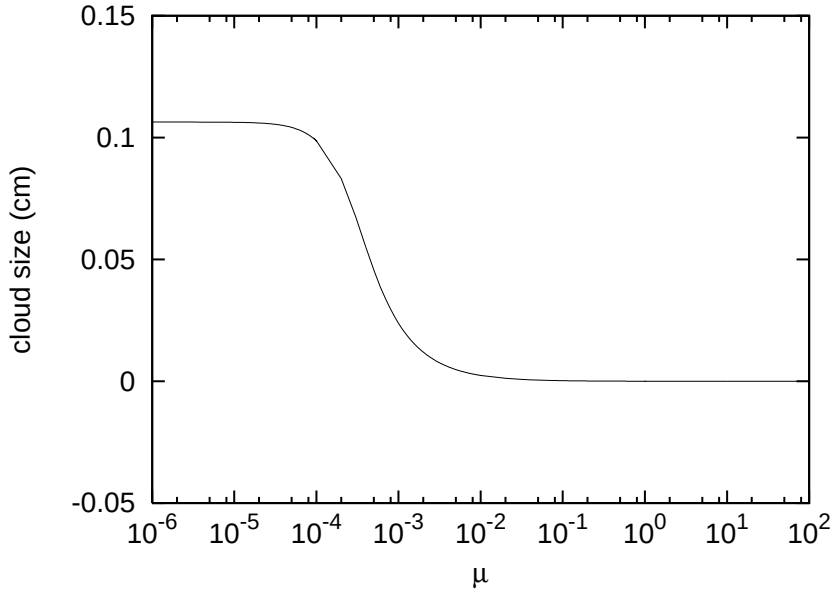

Figure 2.5: Cloud size $1/\sqrt{\alpha}$ as a function of the screening parameter μ for $N = 10^4$ atoms. Coulomb coupling parameter is 10^8. Two limits of the μ dependence is shown. For small values of the screening parameter μ, the cloud size decreases since the screening reduces the range of Coulomb potential. In the opposite limit, as μ goes to zero the value of the cloud size corresponds to that of the bare Coulomb potential, i.e., charged Bose gas.

2.3 Charged Bosons with No Screening

We now consider the situation of a system composed of N identical bosons interacting via the repulsive Coulomb interaction Z^2e^2/r that are confined in an isotropic harmonic trap. As in the case of ultra-cold plasma of ions interacting via the Yukawa potential, we use the Gross-Pitaevskii functional to describe the ground state properties. In dimensionless units introduced previously, the Gross-Pitaevskii energy functional is given by

$$\frac{E}{\hbar\omega} = \frac{1}{2}\int d\mathbf{r_1}\left\{|\nabla\psi(\mathbf{r_1})|^2 + r_1^2|\psi(\mathbf{r_1})|^2\right\} + \gamma\int\int d\mathbf{r_1}d\mathbf{r_2}\frac{|\psi(\mathbf{r_1})|^2|\psi(\mathbf{r_2})|^2}{|\mathbf{r_1}-\mathbf{r_2}|}\,, \tag{2.17}$$

Adapting the Gaussian trial function ansatz as before, the kinetic and external potential energy terms in the energy functional are easily calculated to yield $3N\alpha/2$ and $3N/8\alpha$, respectively. The interaction energy term is calculated by going over to the center-of-mass coordinate system as before, yielding finally

$$E_I = \gamma N^2 \left(\frac{\alpha}{\pi}\right)^{3/2} 4\pi \int_0^\infty r\, dr\, \mathrm{e}^{-\alpha \mathrm{r}^2} = \frac{2\mathrm{N}^2\gamma}{\sqrt{\pi}}\alpha^{1/2}\,. \tag{2.18}$$

The total variational energy is

$$\frac{E}{N\hbar\omega} = \frac{3}{2}\alpha + \frac{3}{8\alpha} + \frac{2N\gamma}{\sqrt{\pi}}\alpha^{1/2}\,. \tag{2.19}$$

Minimizing the energy with respect to α, we get

$$\frac{3}{2} - \frac{3}{8}\alpha^{-2} + \frac{N\gamma}{\sqrt{\pi}}\alpha^{-1/2} = 0\,. \tag{2.20}$$

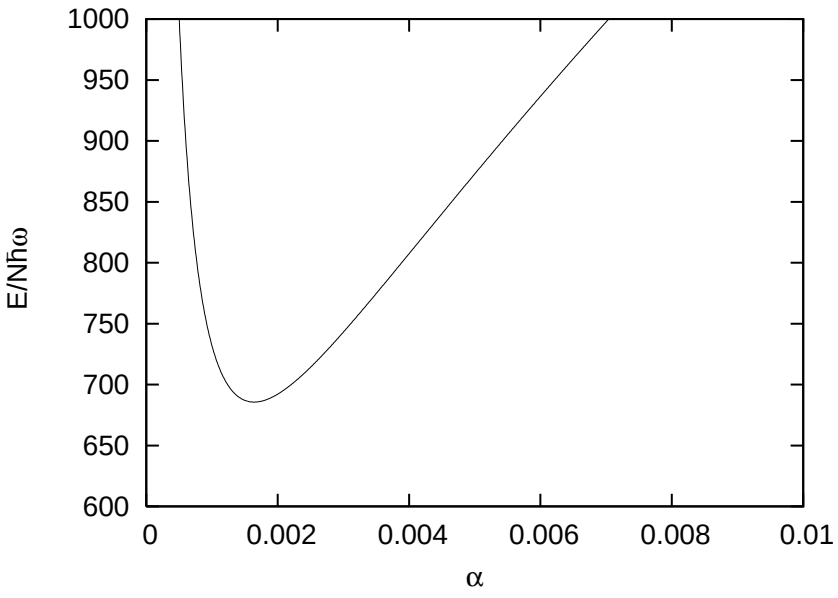

Figure 2.6: Total energy per particle in units of $\hbar\omega$ as a function of variational parameter α for $N = 10^4$ atoms for the bare Coulomb potential. The Coulomb coupling parameter is $\gamma = 1$.

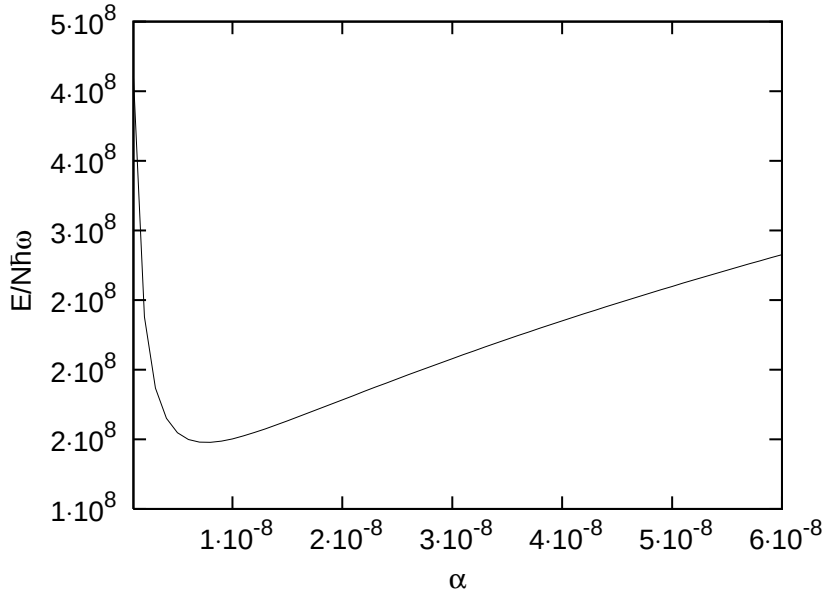

Figure 2.7: Total energy per particle in units of $\hbar\omega$ as a function of variational parameter α for $N = 10^4$ atoms for the bare Coulomb potential The Coulomb coupling parameter is $\gamma = 10^8$.

Figure 2.6 shows the α dependence of the total energy per particle in units of $\hbar\omega$ for $N = 10^4$ atoms and $\gamma = 1$. Figure 2.7 also shows the same dependence for the experimental parameters of Chen *et al.* [47] where the coupling parameter is $\gamma = 10^8$. One can easily see the energy minimum in both curves despite the huge difference in the coupling strength values. Similarly to the Yukawa potential case, we obtain the cloud size for the bare Coulomb potential case as $\sim 2\,\mathrm{mm}$ where the trap frequency is approximately $10^4\,\mathrm{Hz}$.

2.4 Theoretical Model for Ion and Electron Densities

The ion cloud is described as a Bose condensed system within the mean-field approximation as in previous sections, but in this case, electron density is not

assumed to be constant. The ground state energy functional for the ions at zero temperature is given by

$$\begin{aligned} E_i[\psi(\mathbf{r})] &= \int d\mathbf{r} \left\{ \frac{\hbar^2}{2m_i} |\nabla\psi(\mathbf{r})|^2 + \frac{1}{2} m_i \omega^2 r^2 |\psi(\mathbf{r})|^2 \right\} \\ &+ Z^2 e^2 \int\int d\mathbf{r} d\mathbf{r}' \frac{|\psi(\mathbf{r})|^2 |\psi(\mathbf{r}')|^2}{|\mathbf{r}-\mathbf{r}'|} \\ &- Ze^2 \int\int d\mathbf{r} d\mathbf{R} \frac{|\psi(\mathbf{r})|^2 n(\mathbf{R})}{|\mathbf{r}-\mathbf{R}|}, \end{aligned} \tag{2.21}$$

where $\psi(\mathbf{r})$ is the condensate wave function, ω is the harmonic trap frequency, and $n(\mathbf{r})$ is the electron density. We assume that bosonic ions and electrons interact via the bare Coulomb potential. Energy functional is minimized by

$$\delta\{E_i - \mu_i \int |\psi(\mathbf{r})|^2 d\mathbf{r}\} = 0, \tag{2.22}$$

where μ_i the chemical potential subject to the normalization condition $N_i = \int |\psi(\mathbf{r})|^2 d\mathbf{r}$. By functional minimization of energy functional, one can obtain the Gross-Pitaevskii equation as

$$\begin{aligned} \left[-\frac{\hbar^2}{2m_i}\nabla^2 + \frac{1}{2} m_i \omega r^2 + Z^2 e^2 \int d\mathbf{r}' \frac{|\psi(\mathbf{r}')|^2}{|\mathbf{r}-\mathbf{r}'|} \right. \\ \left. - Ze^2 \int d\mathbf{R} \frac{n(\mathbf{R})}{|\mathbf{r}-\mathbf{R}|} \right] \psi(\mathbf{r}) = \mu_i \psi(\mathbf{r}). \end{aligned} \tag{2.23}$$

The Thomas-Fermi energy functional for electrons is composed of three terms,

$$\begin{aligned} E^{TF}[n(\mathbf{r})] = T^{TF}[n(\mathbf{r})] - Ze^2 \int\int d\mathbf{r} d\mathbf{R} \frac{n(\mathbf{r})|\psi(\mathbf{R})|^2}{|\mathbf{r}-\mathbf{R}|} \\ + \frac{e^2}{2} \int\int d\mathbf{r} d\mathbf{r}' \frac{n(\mathbf{r}) n(\mathbf{r}')}{|\mathbf{r}-\mathbf{r}'|}. \end{aligned} \tag{2.24}$$

The first term is the kinetic energy and obtained by integrating the kinetic energy density of a homogeneous electron gas, $t_0[n(\mathbf{r})]$,

$$T^{TF}[n(\mathbf{r})] = \int d\mathbf{r}\, t_0[n(\mathbf{r})], \tag{2.25}$$

where $t_0[n(\mathbf{r})]$ is obtained by summing the single-particle energies, $\varepsilon = \hbar^2 k^2 / 2m_e$, up to the Fermi wave vector $k_F = [3\pi^2 n(\mathbf{r})]^{1/3}$

$$t_0[n(\mathbf{r})] = \frac{\hbar^2}{2\pi^2 m_e}\int_0^{k_F} k^4 dk = \frac{3\hbar^2}{10m_e}(3\pi^2)^{2/3} n(\mathbf{r})^{5/3}, \tag{2.26}$$

then the kinetic energy is obtained as

$$T^{TF}[n(\mathbf{r})] = \frac{3\hbar^2}{10m_e}(3\pi^2)^{2/3}\int d\mathbf{r} n(\mathbf{r})^{5/3}. \tag{2.27}$$

The second term is the electrostatic energy of attraction between the ions and the electrons and the last term represents the electron-electron interactions in the system which is approximated by the Coulomb repulsion between electrons. We assume that the electrons are not interacting with the trap. Then the Thomas-Fermi energy functional becomes

$$\begin{aligned} E^{TF}[n(\mathbf{r})] &= \frac{3\hbar^2}{10m_e}(3\pi^2)^{2/3}\int d\mathbf{r} n(\mathbf{r})^{5/3} - Ze^2\int\int d\mathbf{r}d\mathbf{R}\frac{n(\mathbf{r})|\psi(\mathbf{R})|^2}{|\mathbf{r}-\mathbf{R}|} \\ &+ \frac{e^2}{2}\int\int d\mathbf{r}d\mathbf{r}'\frac{n(\mathbf{r})n(\mathbf{r}')}{|\mathbf{r}-\mathbf{r}'|}. \end{aligned} \tag{2.28}$$

The Thomas-Fermi equation is obtained by minimizing the energy functional with respect to the electron density

$$\delta\{E^{TF} - \mu_e\int n(\mathbf{r})d\mathbf{r}\} = 0, \tag{2.29}$$

and $N_e = \int n(\mathbf{r})d\mathbf{r}$,

$$\frac{\hbar^2}{2m_e}(3\pi^2)^{2/3} n(\mathbf{r})^{2/3} - Ze^2\int d\mathbf{R}\frac{|\psi(\mathbf{R})|^2}{|\mathbf{r}-\mathbf{R}|} + e^2\int d\mathbf{r}'\frac{n(\mathbf{r}')}{|\mathbf{r}-\mathbf{r}'|} = \mu_e. \tag{2.30}$$

The total energy functional becomes

$$\begin{aligned} E[\psi(\mathbf{r}), n(\mathbf{r})] &= \int d\mathbf{r}\left\{\frac{\hbar^2}{2m_i}|\nabla\psi(\mathbf{r})|^2 + \frac{1}{2}m_i\omega^2 r^2|\psi(\mathbf{r})|^2\right\} \\ &+ Z^2e^2\int\int d\mathbf{r}d\mathbf{r}'\frac{|\psi(\mathbf{r})|^2|\psi(\mathbf{r}')|^2}{|\mathbf{r}-\mathbf{r}'|} - Ze^2\int\int d\mathbf{r}d\mathbf{R}\frac{|\psi(\mathbf{r})|^2 n(\mathbf{R})}{|\mathbf{r}-\mathbf{R}|} \\ &+ \frac{3\hbar^2}{10m_e}(3\pi^2)^{2/3}\int d\mathbf{r} n(\mathbf{r})^{5/3} + \frac{e^2}{2}\int\int d\mathbf{r}d\mathbf{r}'\frac{n(\mathbf{r})n(\mathbf{r}')}{|\mathbf{r}-\mathbf{r}'|}. \end{aligned} \tag{2.31}$$

Dimensionless units are introduced by making the same transformation as in the previous sections: (i) $\mathbf{r} \to l\mathbf{r}$, where $l = \sqrt{\hbar/m_i\omega}$ is oscillator length, and (ii) the energy is measured in units of $\hbar\omega$.

The energy functional can now be rewritten using the dimensionless quantities

$$\frac{E}{\hbar\omega} = \frac{1}{2}\int d\mathbf{r}\left\{|\nabla\psi(\mathbf{r})|^2 + r^2|\psi(\mathbf{r})|^2 + \frac{3(3\pi^2)^{2/3}}{5}\frac{m_i}{m_e}n(\mathbf{r})^{5/3}\right\}$$
$$+ \quad \gamma\int\int d\mathbf{r}d\mathbf{r}'\left\{\frac{|\psi(\mathbf{r})|^2|\psi(\mathbf{r}')|^2}{|\mathbf{r}-\mathbf{r}'|} - \frac{1}{Z}\frac{|\psi(\mathbf{r})|^2 n(\mathbf{r}')}{|\mathbf{r}-\mathbf{r}'|} + \frac{1}{2Z^2}\frac{n(\mathbf{r})n(\mathbf{r}')}{|\mathbf{r}-\mathbf{r}'|}\right\} \quad (2.32)$$

where $\gamma = (Ze)^2\sqrt{m_i/\hbar\omega}/\hbar$ is the electrostatic coupling constant. Similarly,

$$\left[-\nabla^2 + r^2 + 2\gamma\int d\mathbf{r}'\frac{|\psi(\mathbf{r}')|^2}{|\mathbf{r}-\mathbf{r}'|} - \frac{2\gamma}{Z}\int d\mathbf{r}'\frac{n(\mathbf{r}')}{|\mathbf{r}-\mathbf{r}'|}\right]\psi(\mathbf{r}) = 2\mu_i\psi(\mathbf{r}), \quad (2.33)$$

and

$$\frac{(3\pi^2)^{2/3}}{2}\frac{m_i}{m_e}n(\mathbf{r})^{2/3} - \frac{\gamma}{Z}\int d\mathbf{r}'\frac{|\psi(\mathbf{r}')|^2}{|\mathbf{r}-\mathbf{r}'|} + \frac{\gamma}{Z^2}\int d\mathbf{r}'\frac{n(\mathbf{r}')}{|\mathbf{r}-\mathbf{r}'|} = \mu_e, \quad (2.34)$$

are the equations satisfied by the condensate wavefunction $\psi(\mathbf{r}')$ and the electron density $n(\mathbf{r}')$.

To find the density distributions, we employ a modified Thomas-Fermi model [44]. We assume spherically symmetric density distributions. If the electrostatic potential arising from electron-ion and ion-ion interactions is called ϕ, the equations of motion become

$$\frac{(3\pi^2)^{2/3}}{2}\frac{m_i}{m_e}n(\mathbf{r})^{2/3} - \frac{\gamma}{Z}\phi = \mu_e, \quad (2.35)$$

and

$$\frac{r^2}{2} + \gamma\phi = \mu_i. \quad (2.36)$$

Substituting ϕ from the latter into the former, the electron density is obtained as

$$n(\mathbf{r}) = \frac{1}{3\pi^2}\left[\frac{2m_e}{Zm_i}\right]^{3/2}\left[Z\mu_e + \mu_i - \frac{r^2}{2}\right]^{3/2}. \quad (2.37)$$

Making use of the Poisson equation

$$\nabla^2\phi = -4\pi[|\psi(\mathbf{r})|^2 - n(\mathbf{r})/Z], \quad (2.38)$$

one gets the ion density as

$$|\psi(\mathbf{r})|^2 = \frac{1}{3\pi^2 Z}\left[\frac{2m_e}{Zm_i}\right]^{3/2}\left[Z\mu_e + \mu_i - \frac{r^2}{2}\right]^{3/2} + \frac{3}{4\pi\gamma}. \quad (2.39)$$

Charge neutrality of the plasma requires $ZeN_i - eN_e = 0$. After normalization we get

$$n(\mathbf{r}) = \frac{2\sqrt{2}N_e}{\pi^2(Z\mu_e + \mu_i)^3}\left[Z\mu_e + \mu_i - \frac{r^2}{2}\right]^{3/2}, \tag{2.40}$$

and

$$|\psi(\mathbf{r})|^2 = \frac{N_i\left\{\frac{1}{3\pi^2 Z}\left[\frac{2m_e}{Zm_i}\right]^{3/2}\left[Z\mu_e + \mu_i - \frac{r^2}{2}\right]^{3/2} + \frac{3}{4\pi\gamma}\right\}}{\left[\frac{(Z\mu_e+\mu_i)^3}{6\sqrt{2}Z}\left[\frac{2m_e}{Zm_i}\right]^{3/2} + \frac{2^{3/2}(Z\mu_e+\mu_i)^{3/2}}{\gamma}\right]}. \tag{2.41}$$

Figure 2.8 shows the density distributions for electrons and ions for $N_e = N_i = 10^4$ and coupling parameter $\gamma = 10^8$. Gaussian density for the ions and constant density for electron that we used in the previous section are shown in the figure also. One can see that electron and ion densities are completely the same. This implies the complete screening of the plasma.

We find the cloud size for the system by using the same parameters that we used before. The cloud size becomes approximately $14\,\mu m$ for 10^4 electrons and 10^4 ions confined with a trapping frequency 10 KHz.

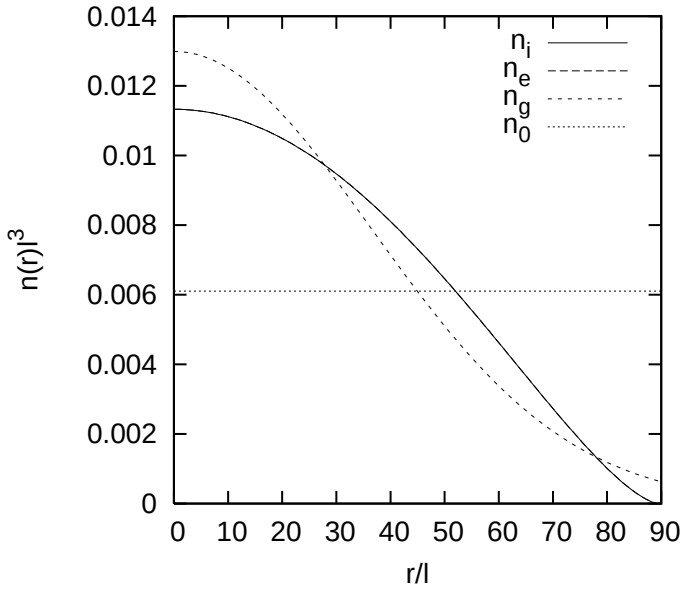

Figure 2.8: Density distributions as a function of r/l where l is oscillator length. Coupling parameter $\gamma = 10^8$ and $N_e = N_i = 10^4$. Gaussian density for the ions n_g and constant electron density n_0 used in [41] is also shown. Electron and ion densities are completely the same.

Chapter 3

Localization of an Impurity Particle on a Boson Mott Insulator Background

The system of ultra-cold atoms in optical lattices can be used to mimic traditional problems in solid-state physics because these systems are highly controllable and experimentally achievable [10, 48–52]. For example, superfluid-Mott insulator phase transition, which is predicted by Bose-Hubbard model, has been experimentally demonstrated in the cold atom optical lattices [10]. With improvement over the control of the system parameters, as well as advancement of measurement techniques such as noise correlations [53], it seems conceivable that a great variety of models will be realized in optical lattices.

Optical lattices are created by overlapping of two counterpropagating laser beams. Atoms are trapped in the optical standing waves which are caused by the interference between the laser beams. The ground-state single-particle wave function is a Bloch wave function for the atoms in a periodic potential. Thus, the Bloch state with zero quasi-momentum, $q = 0$, is macroscopically occupied, when a condensate is loaded in an optical lattice.

Bose-Hubbard (BH) Hamiltonian of the solid state physics totally describe the system of bosonic atoms with repulsive interaction in a periodic potential, as

realized by Jaksch *et al.* [11]

$$H = -t \sum_{<i,j>} b_i^\dagger b_j + \frac{U}{2} \sum_i n_i(n_i - 1), \tag{3.1}$$

where $b^\dagger, b$ are the bosonic creation and annihilation operators respectively; $n_i = b_i^\dagger b_i$ is the on-site number operator for the bosons and the indices $< i, j >$ run over the nearest neighbor sites. The first term in the BH Hamiltonian describes the tunneling of the atoms between neighbouring sites, and second term is for the on-site repulsive interaction.

Depending on the ratio between the the tunnelling strength and the interaction for bosons, the system may either form a superfluid (SF) or a Mott insulator (MI) state [54]. For the case of zero on-site interaction, $U = 0$, the many-body ground-state is an ideal Bose-Einstein condensate where all atoms are in the Bloch states of the lowest band, and each atom is spread out over the entire lattice. In the opposite limit, i.e. $t = 0$, ground-state is a product of local number states with equal number of atoms per site. This ratio between the interaction and the kinetic energy can be varied by simply changing the lattice depth in the experiments [55].

Another new class of quantum models realized by cold gas experiments is the mixture of different species of atoms [56], namely, the boson-boson and boson-fermion mixtures have been created. It is now also possible to selectively turn on optical lattice potentials for any of the species forming the mixture [57]. The experimental realization of atomic gas mixtures stimulated a lot of theoretical interest [58–64]. There are possibilities of pairing due to mediated interactions [59], formation of composite particles similar to molecules [62], large counterflows of different species or even countersuperfluidity [61]. There are also ideas to simulate random potentials using one species as the disorder potential for the others [63]. The parameter space for mixtures is very large, with many possible phases and a complicated phase diagram [62, 64]. Two recent experiments about boson-fermion mixtures have shown that the optical lattice experiments are advanced enough to test these theoretical ideas in the laboratory [65, 66].

In this chapter, we investigate the limit where one bosonic species interacts

with a single fermionic particle [67]. The identity of the external particle does not matter and all the results obtained are valid for a bosonic impurity as well. We assume that both species share the same lattice potential and that the lattice potential is deep enough so that only one band of the lattice is populated. The Hubbard-type Hamiltonian [11] for this system can be written as

$$\begin{aligned} H = & - t_b \sum_{<i,j>} b_i^\dagger b_j + \frac{U_{bb}}{2} \sum_i n_i(n_i - 1) - \mu_b \sum_i n_i \\ & - t_f \sum_{<i,j>} f_i^\dagger f_j + U_{bf} \sum_i n_i f_i^\dagger f_i, \end{aligned} \tag{3.2}$$

where $b^\dagger, b$ and $f^\dagger, f$ are the bosonic and impurity creation and annihilation operators respectively; $n_i = b_i^\dagger b_i$ is the on-site number operator for the bosons and $< i, j >$ represents a sum over nearest neighbors. The strength of the tunnelling terms are characterized by hopping matrix elements t_b for bosons and t_f for the fermion. U_{bb} and U_{bf} are the on-site interaction strengths between bosons and between a boson and a fermion respectively.

The localization problem can be studied in both SF and MI regimes, but we can provide exact results only for the Mott insulator case. Thus, we first consider the exactly solvable case, namely when $t_b/U_{bb} = 0$. For a Mott insulator with n_0 bosons per site, the chemical potential is constrained to

$$U_{bb}(n_0 - 1) \leq \mu_b \leq U_{bb} n_0. \tag{3.3}$$

With these considerations for bosons, the fermion can show two qualitatively different behaviors. It can either behave like a free fermion with its wavefunction stretching throughout the system, or it may create a defect in the Mott insulator and form a bound state with this defect. We calculate the critical interaction strength that separate these two regimes.

3.1 Localization in a Perfect Mott Insulator

In this section, we calculate the critical interaction strength for bound state (polaron) formation in the limit that the boson Mott insulator is perfect, i.e.

the hopping strength for bosons is zero ($t_b/U_{bb} = 0$). When boson hopping is neglected the Mott insulator background becomes almost inert for the fermion, presenting a spatially independent mean field energy shift. In this case, the fermion will move with the dispersion relation

$$E_k = t_f\Big[6 - 2\sum_{i=x,y,z}\cos(k_i a)\Big], \tag{3.4}$$

where $-\pi/a < k_i \leq \pi/a$ is the crystal momentum of the fermion in the i direction and a is the lattice constant. It cannot be expected that this delocalized behavior of the fermion continues if the interactions between the background bosons and the fermion become very strong. For the case of attractive interaction between bosons and the fermion, i.e. $U_{bf} < 0$, it would be energetically favorable to put more bosons at a lattice site and bind the fermion to these bosons. This will only happen at a critical interaction strength, beyond which the energy gained by boson-fermion attraction is larger than the sum of the kinetic energy cost of localizing the fermion and the interaction energy cost of introducing more bosons.

This critical interaction strength can then be found by investigating the single particle Hamiltonian

$$H = -t_f\sum_{<i,j>} f_i^\dagger f_j - V f_0^\dagger f_0, \tag{3.5}$$

where we take the site at which the defect is formed as the origin and assume that the defect represents a localized attractive potential $-V$ to the fermion. The value of V for having a bound state is important for our analysis. This is the discrete version of the problem of existence of a bound state for a localized potential well [44]. Just like the continuum version, in one and two dimensional lattices there is a bound state for an infinitesimally small attractive potential. In three dimensions, however, there is a certain critical value below which there is no bound state. In the case of a finite attractive potential, the dispersion relation takes the following implicit form

$$\phi_k[\tilde{E} + 2\sum_i \cos(k_i a)] = -\tilde{V}\psi_0, \tag{3.6}$$

where $\tilde{E} = E/t_f$ and $\tilde{V} = V/t_f$ are the scaled quantities and $\phi_k = \sum_i \psi_i e^{-i\mathbf{k}\cdot\mathbf{r_i}}$ is the Fourier transform of the particle's wave function. We obtain the relation between the binding energy and the attractive potential by taking the Fourier transform of Equation 3.6

$$\frac{1}{\tilde{V}} = \int_{-\pi}^{\pi}\int_{-\pi}^{\pi}\int_{-\pi}^{\pi} \frac{d\theta_x d\theta_y d\theta_z}{(2\pi)^3} \frac{1}{(6 - 2\sum_i \cos\theta_i) + \epsilon}, \tag{3.7}$$

where $\theta_i = k_i a$ and we take

$$\tilde{E} = -6 - \epsilon, \tag{3.8}$$

with $\epsilon > 0$ being the binding energy. When $\epsilon = 0$, i.e. at the localization threshold, the above integral can be evaluated exactly [68] and the critical value at which the localization takes place is

$$\tilde{V_c} = \frac{2}{(18 + 12\sqrt{2} - 10\sqrt{3} - 7\sqrt{6})\left[\frac{2}{\pi}K(k_0)\right]^2} = 3.95678, \tag{3.9}$$

where $k_0^2 = [(2-\sqrt{3})(\sqrt{3}-\sqrt{2})]^2$ and K is the complete elliptic integral of the first kind. For nonzero ϵ, the integral was evaluated by Joyce [69]. Using this result, the potential is obtained as

$$\tilde{V} = \frac{2}{\frac{(1-\eta)^{1/2}}{\omega}\left(1 - \frac{1}{4}\eta\right)^{1/2}\left(\frac{2}{\pi}\right)^2 K(k_+)K(k_-)}, \tag{3.10}$$

where $\eta = -16z(\sqrt{1-z} + \sqrt{1-9z})^{-2}$, $z = 1/\omega^2 = 1/(3+\epsilon/2)^2$, and $k_\pm^2 = \frac{1}{2}\left[1 \pm \eta\sqrt{1 - \frac{1}{4}\eta} - \left(1 - \frac{1}{2}\eta\right)\sqrt{1-\eta}\right]$. In the limit of large binding energy, $\epsilon >> 1$, we obtain a linear relation $\tilde{V} \propto \epsilon$, which is expected as the particle is strongly localized at a single lattice site.

The exact evaluation of the integral above allows us to calculate not only the critical boundary but also the binding energy $\epsilon(V/t_f)$ of the bound state (Figure 3.1). We now generalize our one particle results to the many particle case. We first assume that the fermion-boson interaction is attractive, $U_{bf} < 0$. In this case, the simplest defect would be to introduce one more boson, thus the attractive potential seen by the fermion will be $V = |U_{bf}|$. However, to introduce one more boson to a Mott insulator with n_0 particles per lattice site would cost

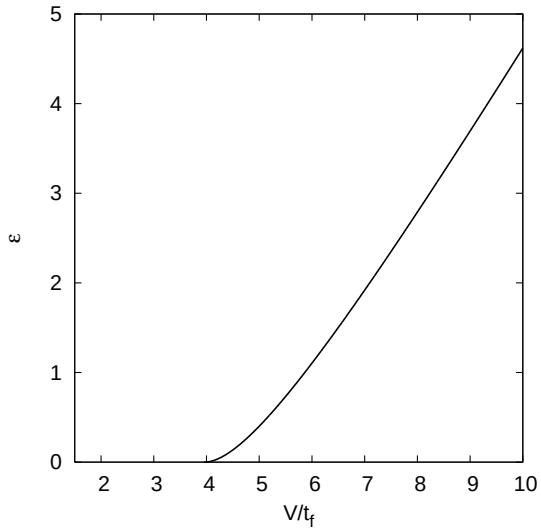

Figure 3.1: Binding energy ϵ of the impurity as a function of V/t_f. The critical interaction strength where the localization begins can also be obtained from the figure, i.e. $\epsilon = 0$ for $V_c/t_f \approx 3.96$.

energy, $U_{bb}n_0 - \mu$. Thus, the phase boundary between the free fermion state and the bound state of the fermion and one bosonic defect (polaron) is given by

$$\epsilon\left(\frac{-U_{bf}}{t_f}\right) = \frac{U_{bb}n_0 - \mu}{t_f}. \tag{3.11}$$

This is not the only defect that can be created in the Mott insulator. If the boson-fermion attraction is strong enough, it becomes energetically favorable to attract more bosons and form a bound state of two bosons and one fermion. The phase boundary for such a defect can be decided by comparing the energy of this state with the energy of the bound state of one boson and one fermion. Thus, the equation for phase boundary is

$$\epsilon\left(\frac{-U_{bf}}{t_f}\right) - \frac{U_{bb}n_0 - \mu}{t_f} = \epsilon\left(\frac{-2U_{bf}}{t_f}\right) - \frac{U_{bb}(2n_0+1) - 2\mu}{t_f}. \tag{3.12}$$

One can similarly find the boundaries for bound states with higher number of bosons.

Another kind of defect is possible for repulsive interactions, i.e. $U_{bf} > 0$. For sufficiently strong repulsive interactions it would be preferable to create a hole in

the Mott insulator state and bind the fermion to this hole. The corresponding phase boundary is given by

$$\epsilon\left(\frac{U_{bf}}{t_f}\right) = \frac{-U_{bb}(n_0-1)+\mu}{t_f}. \tag{3.13}$$

Similar to the attractive interactions, it is possible to form bound states of the fermion with more holes. One can continue to deplete the Mott state until all the n_0 bosons are removed from the defect site. After this point it would be preferable to deplete bosons from the neighboring sites. We have, however, not included such states in our phase diagram. In Figures 3.2, 3.3, and 3.4, we present three phase diagrams for three different values of the chemical potential. Figure 3.2 indicates that when $\mu = (n_0 - 1/2)U_{bb}$, phase diagram is symmetric around $U_{bf} = 0$. This is expected as this value of μ corresponds to lobe centers of the Bose-Hubbard phase diagram where there is particle-hole symmetry. One can also notice from this diagram that when U_{bb} is close to zero, even for small $|U_{bf}|$ values, the fermion can be bound to a large number of bosons. If we take $\mu = (n_0 - 1/4)U_{bb}$ as in Figure 3.3, the symmetry around $U_{bf} = 0$ is broken and for the repulsive interactions it is harder to attract holes. Figure 3.4 represents the opposite case, $\mu = (n_0 - 3/4)U_{bb}$, where stronger interactions are required to attract particles.

We believe that the phase diagram can be checked experimentally. While it would be possible to modify U_{bf} by an interspecies Feshbach resonance, an easier route would be to change t_f which is controlled by the strength of the optical lattice. The localized impurity states can be distinguished from free fermion states as their mean field shifts would be different; in principle, RF spectroscopy [70, 71] would directly detect the difference in the mean field shift. Although the calculation was carried out for a single impurity, we expect these results to be quantitatively correct for a small density of fermionic impurities over a bosonic Mott insulator background. Essentially, if the inverse of Fermi momentum is much larger than the lattice spacing, then the fermions would hardly effect each other's behavior.

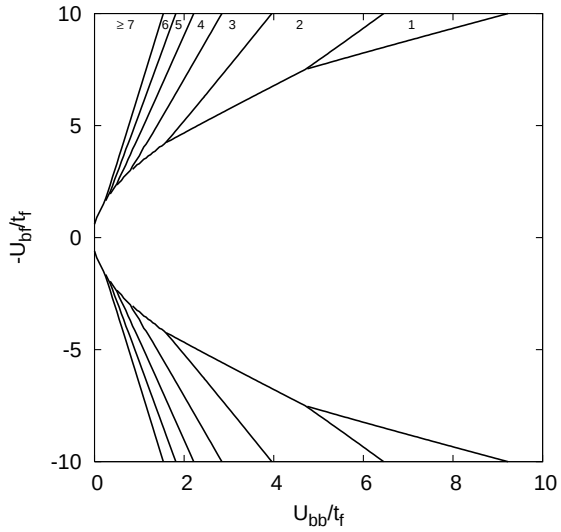

Figure 3.2: Phase diagram for $\mu = (n_0 - 1/2)U_{bb}$. Numbers in each region show how many extra particles ($U_{bf} < 0$) or holes ($U_{bf} > 0$) are attracted to the localization site. The region marked as ≥ 7 contains all the phases with seven or more extra bosons (holes). Phase diagram for this value of μ is symmetric around $U_{bf} = 0$. For small boson-boson repulsion U_{bb}, even for small $|U_{bf}|$ values, large number of bosons are attracted. While this phase diagram is independent of n_0, the number of holes that are attracted is limited by n_0.

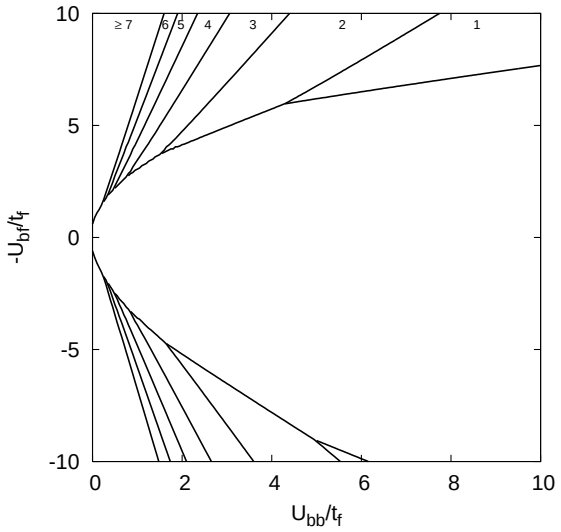

Figure 3.3: Phase diagram for $\mu = (n_0 - 1/4)U_{bb}$. Symmetry in Figure 3.2 is broken and particle attraction is easier than the hole attraction, since the chemical potential is increased with respect to the symmetry point. To attract a hole one needs higher boson-fermion interaction $|U_{bf}|$ for the same U_{bb}.

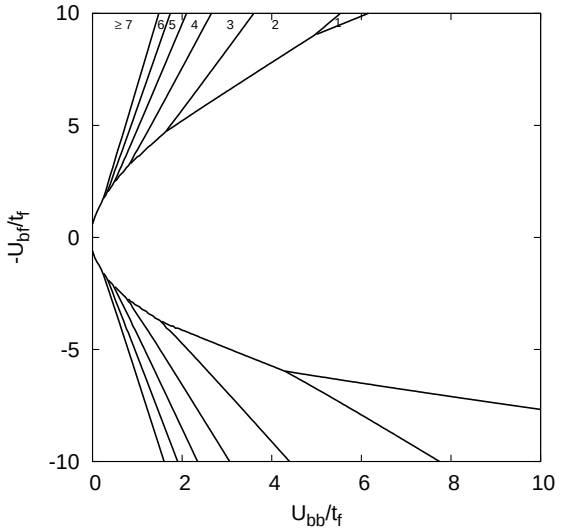

Figure 3.4: Phase diagram for $\mu = (n_0 - 3/4)U_{bb}$. As opposed to Figure 3.3, to attract a particle one needs higher boson-fermion interaction.

3.2 Effects of Lattice Anisotropy

In the optical lattice experiments, it is possible to change the strength of the laser beams forming the lattice, hence realize a model system where the lattice is not isotropic. We assume that the hopping strength for the fermion is different in one direction compared to the other two directions and calculate the effect of such anisotropy on the phase diagram of the previous section. The localization threshold for the anisotropic case can also be calculated analytically. Thus, in the following discussion we need not assume that the anisotropy of the lattice is small.

Because of the anisotropy, the single particle Hamiltonian in Equation 3.5 is modified as

$$H = -t_f \sum_{<i,j>} f_i^\dagger f_j - t'_f \sum_{<i,j>} f_{iz}^\dagger f_{jz} - V f_0^\dagger f_0, \tag{3.14}$$

where we take the hopping term in the z direction to be $t'_f \neq t_f$. We obtain the relation between $\tilde{V}$ and ϵ as

$$\frac{1}{\tilde{V}} = \int_{-\pi}^{\pi}\int_{-\pi}^{\pi}\int_{-\pi}^{\pi} \frac{d\theta_x d\theta_y d\theta_z}{(2\pi)^3} \frac{1}{[4 - 2\sum_{i=x,y}\cos\theta_i + 2\tau(1-\cos\theta_z)] + \epsilon}, \tag{3.15}$$

where $\tilde{E} = -4 - 2\tau - \epsilon$ and $\tau = t'_f/t_f$. For $\epsilon = 0$ this integral can be evaluated exactly [68]. The critical value for the localization is found to be

$$\tilde{V}_c = \frac{2}{\frac{\sqrt{2}}{\tau}(\sqrt{2}\sqrt{1+\tau} - \sqrt{2+\tau})\left(\frac{2}{\pi}\right)^2 K[k_+(\tau)]K[k_-(\tau)]}, \tag{3.16}$$

where

$$k_\pm(\tau)^2 = \left[\frac{1}{\tau}(\sqrt{2}\sqrt{1+\tau} - \sqrt{2+\tau})(\sqrt{2+\tau} \pm \sqrt{2})\right]^2. \tag{3.17}$$

As τ increases, i.e. the anisotropy of the lattice increases, the critical value for the potential increases and the localization becomes more difficult (Figure 3.5). As $t'_f \to 0$, the system becomes two dimensional and there is no threshold for localization, as expected. For large t'_f/t_f, $V_c \sim \sqrt{t'_f t_f}$, which gives $V_c \to 0$ in the one dimensional limit, $t_f \to 0$. Moreover, it is possible to evaluate the integral for nonzero ϵ [68], yielding

$$\tilde{V} = \frac{2(\sqrt{1-(2-\tau)^2 z} + \sqrt{1-(2+\tau)^2 z})}{w\left(\frac{2}{\pi}\right)^2 K[k_+(\tau)]K[k_-(\tau)]}, \tag{3.18}$$

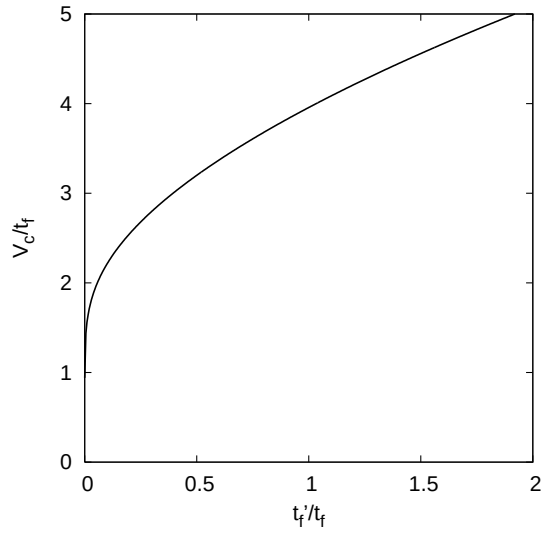

Figure 3.5: The critical value of interaction V_c/t_f as a function of lattice anisotropy characterized by t'_f/t_f (Equation 3.16). If the hopping parameter t'_f increases, anisotropy of the lattice increases and the localization becomes more difficult. $\tau = t'_f/t_f = 1$ gives V_c/t_f for the isotropic case.

where $w = 2 + \tau + \epsilon/2$, $z = 1/w^2$ and

$$
\begin{aligned}
k_{\pm}^2 &= \frac{1}{2} - \frac{1}{2}\left[\sqrt{1-(2-\tau)^2 z} + \sqrt{1-(2+\tau)^2 z}\right]^{-3} \\
&\times \left[\sqrt{1+(2-\tau)\sqrt{z}}\sqrt{1-(2+\tau)\sqrt{z}} + \sqrt{1-(2-\tau)\sqrt{z}}\sqrt{1+(2+\tau)\sqrt{z}}\right] \\
&\times \left\{\pm 16z + \sqrt{1-\tau^2 z}\left[\sqrt{1+(2-\tau)\sqrt{z}}\sqrt{1+(2+\tau)\sqrt{z}}\right.\right. \\
&+ \left.\left.\sqrt{1-(2-\tau)\sqrt{z}}\sqrt{1-(2+\tau)\sqrt{z}}\right]^2\right\}.
\end{aligned}
\tag{3.19}
$$

Using this exact result, the phase diagram can be obtained for arbitrary τ. In Figure 3.6, we display the phase diagram for $\tau = 1.5$. Comparing Figure 3.6 with Figure 3.2 (isotropic case) we see that the phase boundaries are closer to the U_{bf} axis.

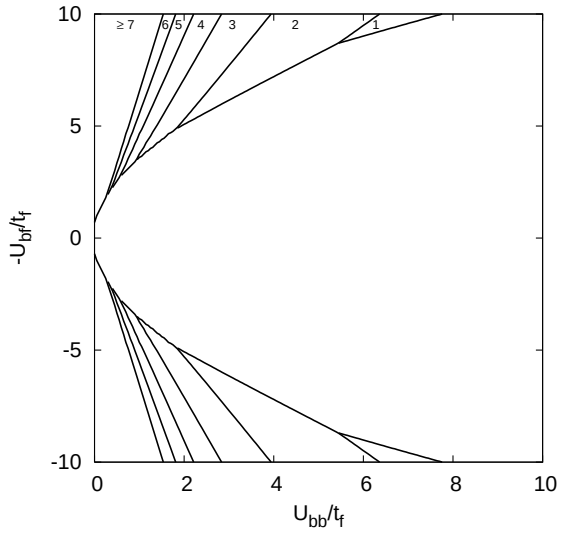

Figure 3.6: Phase diagram in the presence of lattice anisotropy (for $\tau = t'_f/t_f = 1.5$ and $\mu = (n_0 - 1/2)U_{bb}$). To be compared with Figure 3.2 ($\tau = 1$, $\mu = (n_0 - 1/2)U_{bb}$). One can see that anisotropy with $\tau > 1$ causes the localization threshold to move to higher values of $|U_{bf}|$.

3.3 Effects of Higher Impurity Bands

An important point one always has to keep in mind that the effective Hubbard models, such as Equation 3.5, are obtained by projecting the system into the lowest band of the lattice [11]. This procedure is expected to describe the low energy physics as long as the band gaps are larger than the temperature and interaction scales in the problem. In the equivalent language of Wannier functions, this condition corresponds to requiring the Wannier function of each lattice site to be undisturbed by interactions.

In the context of the current problem, we discussed the critical hopping strength that is needed to localize the impurity particle to a small region, which is of the order of one lattice site. The precise determination of the Hubbard model parameters such as U_{bf} depends on the microscopic model one starts from. For the Hubbard model to work correctly, the Wannier functions for the impurity must be unchanged even if the impurity particle is localized to one lattice site. As a localized impurity attracts (or repels) extra particles (holes) to its localization

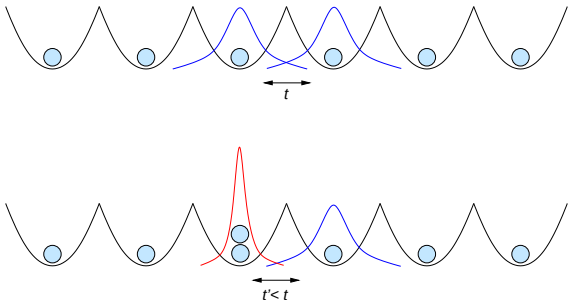

Figure 3.7: Schematic representation of the effect of higher impurity bands to the hopping parameter. If the localized impurity attracts extra particles (holes) to the localization site, the local wave function of the impurity particle changes. Then the hopping parameter for this site is different from that for the other sites.

site, one may expect the on-site wave function of the localized particle to be different from the Wannier functions at other lattice sites. This is essentially considering the coupling of the localized particle to higher impurity bands, and should be a small effect controlled by the parameter $\frac{U_{bf}}{\Delta_f}$, where Δ_f is the width of the first band gap of the impurity bands. Thus, the effect we are considering in this section would be important only if the impurity particle is highly mobile in the lattice, while the interaction between the background particles and the impurity is strong enough to localize the particle (Figure 3.7).

In such a case, the system can still be modelled by a Hubbard model where the hopping strength between the localization site and its neighbors (t'_f) is different from the hopping strength between any other neighboring sites in the lattice (t_f). These hopping strengths can once again be calculated by looking at the overlaps of the localized wavefunctions between neighboring lattice sites [11].

In this case, we take the single particle Hamiltonian as

$$H = -t_f \sum_{<i,j>} f_i^\dagger f_j - (t'_f - t_f) \sum_{<l,m>} f_l^\dagger f_m (\delta_{l0} + \delta_{m0}) - V f_0^\dagger f_0. \tag{3.20}$$

Calculations similar to those performed in the previous sections yield

$$\tilde{V} = \frac{1 - \int_{-\pi}^{\pi}\int_{-\pi}^{\pi}\int_{-\pi}^{\pi} \frac{d\theta_x d\theta_y d\theta_z}{(2\pi)^3} \frac{2(\tau-1)\sum_i \cos\theta_i}{6-2\sum_i \cos\theta_i + \epsilon}}{\int_{-\pi}^{\pi}\int_{-\pi}^{\pi}\int_{-\pi}^{\pi} \frac{d\theta_x d\theta_y d\theta_z}{(2\pi)^3} \frac{1}{6-2\sum_i \cos\theta_i + \epsilon}}, \tag{3.21}$$

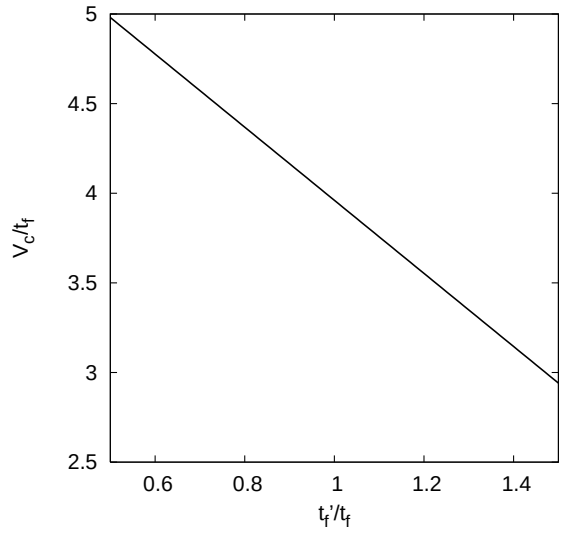

Figure 3.8: The critical value of interaction V_c/t_f as a function of $\tau = t'_f/t_f$ (Equation 3.23). As the ratio of the hopping parameters τ increases, localization occurs for smaller values of the interaction.

where $\tilde{E} = -6 - \epsilon$. Evaluating this integral exactly [72], we obtain the relation

$$\tilde{V} = \frac{2\tau}{\frac{(1-\eta)^{1/2}}{\omega}\left(1-\frac{1}{4}\eta\right)^{1/2}\left(\frac{2}{\pi}\right)^2 K(k_+)K(k_-)} - 2(\tau-1)\omega, \tag{3.22}$$

where $\eta = -16z(\sqrt{1-z}+\sqrt{1-9z})^{-2}$, $z = 1/\omega^2 = 1/(3+\epsilon/2)^2$, and $k_\pm^2 = \frac{1}{2}\left[1 \pm \eta\sqrt{1-\frac{1}{4}\eta} - \left(1-\frac{1}{2}\eta\right)\sqrt{1-\eta}\right]$. When $\epsilon = 0$, the critical value for the potential is found to be

$$\tilde{V_c} \approx 3.95678[1 - 0.51622(\tau - 1)]. \tag{3.23}$$

As can be seen in Figure 3.8, the coupling to higher impurity bands can substantially change the critical value for localization. If $U_{bf} < 0$, we expect a narrowing of the local wave function (as in Figure 3.7), then $t'_f < t_f$ and consequently localization is harder $V_c(\tau) > V_c(\tau = 1)$. Similarly if $U_{bf} > 0$ we expect easier localization. In general one would then expect each different polaron state to have a different τ value. Still to gain a basic understanding of this effect we obtain the phase diagram (Figure 3.9) using constant value of $\tau = 1.5$.

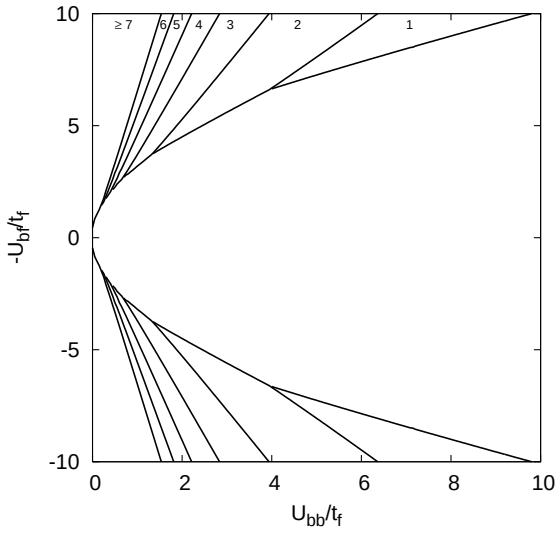

Figure 3.9: Phase diagram obtained when the effect of higher impurity bands is taken into account ($\tau = 1.5$, $\mu = (n_0 - 1/2)U_{bb}$). This effect is modelled by the parameter τ, which is the ratio of the hopping strength between the localization site and its neighbors to the one between any other neighboring sites. Compare this figure with Figure 3.2 ($\tau = 1$, $\mu = (n_0 - 1/2)U_{bb}$). One can see that localization is easier if $\tau > 1$.

Chapter 4

2D Bose-Einstein Condensate with Gravitylike Interatomic Attraction

Investigations of Bose-Einstein condensates (BEC) have been mostly concentrated on systems with short range two-body interaction which is characterized by the s-wave scattering length [14]. Recently, O'Dell *et al.* [12] proposed a configuration for the occurrence of $1/r$ interaction which is a totally new regime for cold gases that have a long-range attractive interaction. They showed that a particular spatial configuration of external electromagnetic fields which generate a $1/r$ potential in the near zone. The analysis of this configuration is important also because it suggests a new way to examine the stellar $1/r$ interaction in the laboratory. Apart from this possibility, it is interesting that such a system results in stable condensates even in the absence of an external trap potential [73]. Recent experiments [77] on polar molecules and condensates with dipole-dipole interactions started to probe the properties of such systems.

In the aforementioned configuration the intense off-resonant laser beams are adjusted so as to cancel the r^{-3} term in the dipole-dipole interaction leaving only the $1/r$ attractive interaction stabilizing the BEC [12]. The fields caused by laser beams induce the dipoles with which the atoms are coupled. The dipole-dipole interaction energy, caused by an external electromagnetic radiation with intensity

I, can be written [12]

$$U(\mathbf{r}) = \left(\frac{I}{4\pi c\varepsilon_0^2}\right)\alpha^2(k)\hat{\mathbf{e}}_i^*\hat{\mathbf{e}}_j V_{ij}(k,\mathbf{r})\cos(\mathbf{k}\cdot\mathbf{r}), \tag{4.1}$$

where $\mathbf{k}$ is the wave vector, $\hat{\mathbf{e}}$ is the polarization vector, $\mathbf{r}$ is the interatomic axis, and $\alpha(k)$ is the dynamic polarizability. Retarded dipole-dipole interaction tensor V_{ij} is

$$V_{ij} = \frac{1}{r^3}[(\delta_{ij} - 3\hat{\mathbf{r}}_i\cdot\hat{\mathbf{r}}_j)(\cos kr + kr\sin kr) - (\delta_{ij} - \hat{\mathbf{r}}_i\cdot\hat{\mathbf{r}}_j)k^3r^2\cos kr], \tag{4.2}$$

where $\hat{\mathbf{r}}_i = r_i/r$. It is assumed that the atoms are not excited by the laser beams. Thirunamachandran [78] noted that the static dipolar part of the interaction, $r^{-3}(\delta_{ij} - 3\hat{\mathbf{r}}_i\hat{\mathbf{r}}_j)$, vanishes by taking the over all average of the interatomic axis with respect to the incident radiation direction. Thus, in the near-zone ($kr \ll 1$), only the attractive $1/r$ potential remains.

O'Dell *et al.* [12] considered a spatial configuration with three orthogonal circularly polarized laser beams, called triads, in the directions $\hat{\mathbf{x}}$, $\hat{\mathbf{y}}$, $\hat{\mathbf{z}}$, to get rid of the r^{-3} term. They showed that this triad configuration gives rise to the following potential, in the near-zone,

$$U(\mathbf{r}) = -\frac{3Ik^2\alpha^2}{16\pi c\varepsilon_0^2}\frac{1}{r}\left[\frac{7}{3} + (\sin\theta\cos\phi)^4 + (\sin\theta\sin\phi)^4 + (\cos\theta)^4\right], \tag{4.3}$$

where (θ,ϕ) is the orientation of $\mathbf{r}$ relative to the laser beams. Then, they obtained a purely radial potential by combining 6 triads with different orientations. Finally, they get the potential as

$$U(\mathbf{r}) = -\frac{11}{4\pi}\frac{Ik^2\alpha^2}{c\varepsilon_0^2}\frac{1}{r} = -\frac{u}{r}. \tag{4.4}$$

By introducing frequency shifts between the laser beams, one can overcome the difficulty of surviving of r^{-3} interaction due to the interference between the beams.

In this system, two new regimes appear where the kinetic energy, contact interaction energy and gravitylike attractive interaction form a stable configuration without a trap potential [12, 79] i.e., the condensate is self-bound. Self-bound condensates have been examined extensively in the literature in the context

of laser induced gravitation [80] and other systems [73–76]. Ghosh [81] has studied the collective excitation frequencies of this system in three-dimensions (3D) within the time-dependent variational method. He showed that variational analysis agrees with the results of Ref. [79] very well in which the sum-rule approach was used. Recently it has been shown that numerical solutions are in very good agreement with the variational solutions for 3D systems [82].

There is a growing interest in condensates with long-range interactions, especially in those with dipole-dipole interaction [83, 84]. After the realization of Bose-Einstein condensation with ^{52}Cr atoms [13], many theoretical and experimental studies on systems with dipolar interaction appeared in the literature [85]. The recent progress on the cooling and trapping of neutral atomic gases with electromagnetic field has also made it possible to study 2D Bose gases [86]. The 2D atomic BECs have many interesting properties as revealed by experiments and theoretical predictions. The excitation spectrum and vortex states of ordinary 2D BECs [87, 88] and BECs with dipole-dipole interaction [89] have also been investigated.

In this chapter we study a 2D condensate with attractive $1/r$ interaction [90]. We calculate the ground-state properties using a variational approach and show that the condensate is stable without an external potential. We also consider the dynamics of the condensate within the time-dependent variational method and calculate the monopole and quadrupole mode frequencies. We examine the excitation spectrum for the Thomas-Fermi gravity and gravity regimes, analyze the vortex states and calculate the coherence length as well as the critical angular frequency to create a vortex. Our work parallels a similar consideration for 3D condensates [81] which allows for a comparison of the effects of dimensionality.

4.1 Ground-state Properties

We will make use of the mean field theory together with the variational method to investigate the ground state properties. For a dilute gas of bosonic atoms, we

can write the equation of motion for the system as,

$$i\hbar\frac{\partial\psi(\mathbf{r},t)}{\partial t} = \left[-\frac{\hbar^2}{2m}\nabla^2 + V_{ext}(\mathbf{r}) + V_H(\mathbf{r})\right]\psi(\mathbf{r},t), \tag{4.5}$$

in which $V_{ext} = m\omega_0^2 r^2/2$ is the external harmonic potential and V_H is the Hartree potential consisting of hard sphere and gravity interactions, respectively, in the form

$$V_H(\mathbf{r}) = g \mid \Psi(\mathbf{r}) \mid^2 -u\int d^2\mathbf{r}'\frac{\mid \Psi(\mathbf{r}') \mid^2}{\mid \mathbf{r}' - \mathbf{r} \mid}, \tag{4.6}$$

where $g = 2\sqrt{2\pi}\hbar^2 a/ma_z$ is the interaction strength with a being the 2D s-wave scattering length, and a_z is the harmonic oscillator length in the tightly confined direction. We consider a highly anisotropic condensate, i.e., $\omega_z \gg \omega_\perp$, and use the quasi-three-dimensional (Q3D) scattering model. In this model, if $a_z \gg a$, atoms experience collisions in 3D and the contact interaction parameter can be written in terms of the same parameter in 3D [91–93]. One should keep in mind that the Hartree potential can be written in this form if the $-u/r$ potential is sufficiently weak and does not affect the short-range scattering. We use the variational wavefunction in the form $\Psi(\mathbf{r},\lambda) = \sqrt{N/\pi\lambda^2 l_0^2}\exp(-r^2/2\lambda^2 l_0^2)$, where $l_0 = \sqrt{\hbar/m\omega_0}$ and this form satisfies the normalization condition with total number of particles N. Using this function in the energy functional, energy per particle can be obtained as

$$\frac{E(\lambda)}{N\hbar\omega_0} = \frac{1}{2}(\lambda^{-2} + \lambda^2 + \tilde{s}\lambda^{-2} - 2\tilde{u}\lambda^{-1}), \tag{4.7}$$

where the dimensionless interaction parameters are $\tilde{s} = \sqrt{2/\pi}Na/a_z$ and $\tilde{u} = \sqrt{\pi/2}uN/(2l_0\hbar\omega_0)$. Equation 4.7 implies that the scattering interaction (third term) in 2D shifts the kinetic energy by $\tilde{s}$. Minimizing the energy with respect to the variational parameter λ, we obtain

$$1 - (1+\tilde{s})\lambda^{-4} + \tilde{u}\lambda^{-3} = 0\,. \tag{4.8}$$

One can obtain the virial relation as $-T + V_{ext} - E_s - E_u/2 = 0$ from a scaling analysis which is equivalent to the above relation, where T and V_{ext} are the kinetic and trap potential energies, E_s and E_u are the interaction energies. It

is worth mentioning here that variational calculations have been shown [82] to be quite accurate for a large range of parameters in the case of 3D condensates with gravitylike interaction. Based on our variational results, Table 4.1 gives the comparison of the four asymptotic regions for some experimental quantities such as the condensate radius, release energy and peak density. The radius and release energy are experimentally important quantities since they are the signatures of $1/r$ interaction [12]. As can be seen from the phase diagram in Figure 4.1(a), there are four regions, as in 3D. Ideal noninteracting region (I) and ordinary Thomas-Fermi region (TF-O) are well-known from the study of ordinary condensates (with short-range interaction only). The gravity (G) and Thomas-Fermi-gravity (TF-G) regions are related to the balance of the gravitylike potential with the kinetic energy and the contact interaction, respectively. Because these regions are not sensitive to the external potential, it can be adiabatically turned off. The gravitylike attraction does not induce the collapse of the condensate unlike the contact interaction. Different from the 3D system [12], a 2D condensate is stable for negative scattering lengths if $\tilde{s} > -1$ irrespective of the value of $\tilde{u}$ whereas there is a sudden collapse for $\tilde{s} \leqslant -1$. In 3D, the condition below which there is no stable condensate becomes $\tilde{s}\tilde{u} \leq 1/4$ [12]. From Figure 4.1(b), one can conclude that self-bound condensate is stable without the external trap. This can also be seen from Equation 4.7, which reveals that for small radii gravitylike attraction is always weaker than the kinetic energy; thus the stability of the condensate depends on the balance between the kinetic energy and the contact interaction.

4.2 Collective Excitations

We use the time-dependent variational approach to obtain the dynamics of the condensate. The Lagrangian density can be written as [94]

$$\mathcal{L} = \frac{i\hbar}{2}\left(\psi\frac{\partial\psi^*}{\partial t} - \psi^*\frac{\partial\psi}{\partial t}\right) - \frac{\hbar^2}{2m}|\nabla\psi|^2 + \frac{V_H(\mathbf{r})}{2}|\psi|^2\,, \tag{4.9}$$

in which the external potential is set to zero. Oscillation frequencies in 3D obtained by a Gaussian ansatz are compatible with the exact calculations [79].

Table 4.1: Comparison of four asymptotic regions.

	G	TF-G	TF-0	I
defn:	$\tilde{u} \gg 1$	$\tilde{s} \ll \tilde{u}^{4/3}$	$\tilde{s} \gg 1$	$\tilde{u} \ll 1$
	$\tilde{s} \ll 1$		$\tilde{s} \gg \tilde{u}^{4/3}$	$\tilde{s} \ll 1$
λ :	$1/\tilde{u}$	$\tilde{s}/\tilde{u}$	$\tilde{s}^{1/4}$	1
$E_{rel}/\hbar\omega_0$:	$\frac{1}{2}N\tilde{u}^2$	$\frac{1}{2}N\tilde{u}^2\tilde{s}^{-1}$	$\frac{1}{2}N\tilde{s}^{1/2}$	$\frac{1}{2}N$
	$\propto N^3$	$\propto N^2$	$\propto N^{3/2}$	$\propto N$
ρ_{max}:	$\frac{N^3u^2}{16l_0^4\hbar^2\omega_0^2}$	$\frac{Na_z^2u^2}{16a^2l_0^4\hbar^2\omega_0^2}$	$\frac{N^{1/2}a_z^{1/2}}{(2\pi^5)^{1/4}a^{1/2}l_0^2}$	$\frac{N}{\pi l_0^2}$

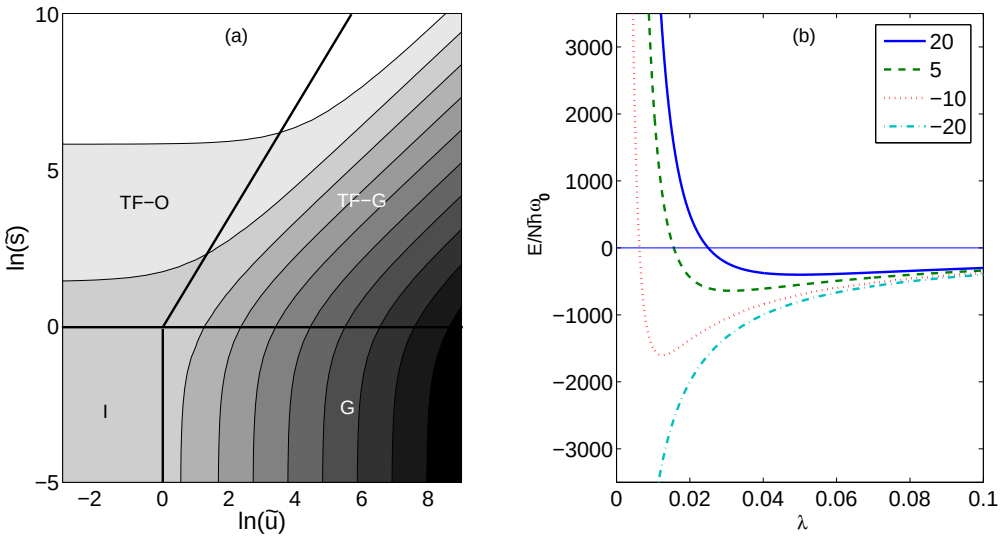

Figure 4.1: (a) Contour plot of the logarithm of the condensate radius as a function of $\ln\tilde{u}$ and $\ln\tilde{s}$, darker shade corresponds to smaller radius. Four asymptotic regions can be seen from the plot. (b) Ground-state energy of the condensate for different values of the variational parameter $\tilde{s}\tilde{u}$ as a function of λ, the condensate radius, for large $\tilde{u}$. The energy is scaled by $N\hbar\omega_0$ and radius is scaled by l_0, the harmonic oscillator length. For $\tilde{s} \leqslant -1$, there is no minimum for finite radius.

Thus, we choose the trial function

$$\psi(x,y,t) = \sqrt{\frac{N}{\alpha_1\beta_1\pi}}\exp\left(-\frac{1}{2}[\alpha(t)x^2+\beta(t)y^2]\right), \tag{4.10}$$

where the wavefunction is normalized to N and x and y are variables in units of $l_0 = \sqrt{\hbar/m\omega_g}$ and $\omega_g = mu^2N^2/\hbar^3$ is the gravitational frequency. $\alpha(t) = 1/\alpha_1^2 + i\alpha_2$ and $\beta(t) = 1/\beta_1^2 + i\beta_2$ are the dimensionless time-dependent variational parameters, and α_1 and β_1 are condensate widths along the x and y directions, respectively. The complex parts of the variational parameters α, β are necessary for an accurate description of the condensate dynamics [95]. Substituting this wavefunction into the Lagrangian density and integrating over 2D spatial coordinates we obtain the following Lagrangian:

$$L = \frac{SN^2u^2}{g}\left[\frac{1}{2}\left(\alpha_1^2\dot{\alpha}_2+\beta_1^2\dot{\beta}_2\right) - \frac{1}{2}\left(\frac{1}{\alpha_1^2}+\alpha_1^2\alpha_2^2\right) - \frac{1}{2}\left(\frac{1}{\beta_1^2}+\beta_1^2\beta_2^2\right)\right.$$
$$\left. - \frac{1}{\pi}\frac{S}{\alpha_1\beta_1} + \sqrt{\frac{\pi}{2}}\frac{{}_2F_1[\frac{1}{2},\frac{1}{2};1;(1-\frac{\beta_1^2}{\alpha_1^2})]}{\alpha_1}\right], \tag{4.11}$$

where $S = gmN/2\hbar^2$ is a dimensionless scattering parameter and ${}_2F_1[1/2,1/2;1;(1-\beta_1^2/\alpha_1^2)]$ is the hypergeometric function. Note that the scattering parameter S in this part is related to the earlier $\tilde{s}$, by $S = \pi\tilde{s}$.

The ground-state energy as a function of the variational parameter in an isotropic system is found to be

$$E = \frac{SN^2u^2}{g}\left[\frac{1}{\alpha^2}+\frac{1}{\pi}\frac{S}{\alpha^2}-\sqrt{\frac{\pi}{2}}\frac{1}{\alpha}\right]. \tag{4.12}$$

Minimizing the energy functional with respect to the variational parameter α, equilibrium point is obtained as $\sigma = (2/\pi)^{1/2}(2+2S/\pi)$. The chemical potential $\mu = \partial E/\partial N$ and sound velocity $c_s^2 = \mu/m$ can be calculated from Equation (4.12). Using the Euler-Lagrange equations, the time evolutions of the widths are

$$\ddot{\alpha_1} = \frac{1}{\alpha_1^3}+\sqrt{\frac{\pi}{2}}\left(\frac{\tilde{S}}{\alpha_1^2\beta_1}+F_{\alpha_1}\right), \tag{4.13}$$

$$\ddot{\beta}_1 = \frac{1}{\beta_1^3} + \sqrt{\frac{\pi}{2}}\left(\frac{\tilde{S}}{\alpha_1\beta_1^2} + F_{\beta_1}\right), \tag{4.14}$$

where $\tilde{S} = \sqrt{2/\pi^3}S$ and F_{α_1}, F_{β_1} are derivatives of ${}_2F_1[1/2, 1/2; 1; 1-\beta_1^2/\alpha_1^2]/\alpha_1$ with respect to α_1 and β_1, respectively. We are looking for low-energy excitations which correspond to small oscillations around the equilibrium point. Thus, we perform an expansion around the equilibrium width by letting $\alpha_1 = \sigma + \delta\alpha_1$ and $\beta_1 = \sigma + \delta\beta_1$ for the isotropic system. The time evolutions of the widths are given by:

$$\delta\ddot{\alpha}_1 = \left[-\frac{3}{\sigma^4} + \sqrt{\frac{\pi}{2}}\left(-\frac{2\tilde{S}}{\sigma^4} + \frac{5}{8\sigma^3}\right)\right]\delta\alpha_1 + \sqrt{\frac{\pi}{2}}\left[-\frac{S}{\sigma^4} + \frac{3}{8\sigma^3}\right]\delta\beta_1, \tag{4.15}$$

$$\delta\ddot{\beta}_1 = \sqrt{\frac{\pi}{2}}\left[-\frac{\tilde{S}}{\sigma^4} + \frac{3}{8\sigma^3}\right]\delta\alpha_1 + \left[-\frac{3}{\sigma^4} + \sqrt{\frac{\pi}{2}}\left(-\frac{2\tilde{S}}{\sigma^4} + \frac{5}{8\sigma^3}\right)\right]\delta\beta_1. \tag{4.16}$$

Substituting $e^{i\omega t}$ type solutions in the above set of equations, we obtain the following excitation frequencies:

$$\omega_+^2 = \frac{3}{\sigma^4} + \sqrt{\frac{\pi}{2}}\left(\frac{3\tilde{S}}{\sigma^4} - \frac{1}{\sigma^3}\right), \tag{4.17}$$

$$\omega_-^2 = \frac{3}{\sigma^4} + \sqrt{\frac{\pi}{2}}\left(\frac{\tilde{S}}{\sigma^4} - \frac{1}{4\sigma^3}\right). \tag{4.18}$$

The excitation spectrum for a 2D condensate with gravitylike interaction is plotted in Figure 4.2 as a function of the dimensionless scattering parameter. We observe that, in contrast to 3D, the 2D system can bear the negative scattering parameter down to $S = -\pi$. For large values of the scattering parameter, the pseudo-potential term dominates the gravitational energy and the monopole mode is more energetic than the quadrupole mode. At $S = 9.42$, there is an intersection of the two modes which can be seen from the inset of Figure 4.2, where it is not possible to distinguish two modes experimentally. A similar crossing occurs in 3D at a larger value of S [81].

TF-G regime: When the gravitylike potential is balanced by the contact interaction i.e., for large s-wave scattering lengths, the kinetic energy can be

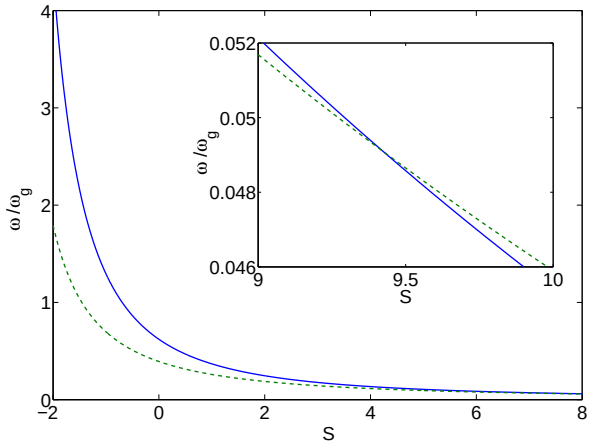

Figure 4.2: Monopole (dashed line) and quadrupole mode (solid line) frequencies (ω_M and ω_Q, respectively) as a function of the dimensionless scattering parameter S. Inset shows the intersect of two modes.

neglected. The total energy of the ground-state becomes $E_0 = -0.62(N^2u^2/g)$. The ground-state energy per particle varies with N as in 3D. In this regime, quadrupole and monopole frequencies are obtained respectively as $\omega_Q = 1.5462\omega_g S^{-3/2}$ and $\omega_M = 2.1867\omega_g S^{-3/2}$. Their ratio is $\omega_M/\omega_Q = 1.42$ which is 1.58 in 3D. Note also that the dependence of ω_Q and ω_M on S in 3D is $\sim S^{-3/4}$ which is a distinctive feature. The facility with which the s-wave scattering length can be tuned through the Feshbach resonance makes the results of our calculation amenable to experimental investigations. The identification of the 2D nature of condensates is thus possible from the study of collective excitations.

G regime: In this regime, we neglect the contact interaction; this is the analog of the nonrelativistic boson star [96]. The ground-state energy per particle varies with N similar to the case in TF-G regime. Quadrupole and monopole mode frequencies are calculated as $\omega_Q = 0.6269\omega_g$ and $\omega_M = 0.3927\omega_g$, respectively, in terms of the gravitational frequency ω_g. Their ratio is $\omega_M/\omega_Q = 0.63$ in this regime which is to be compared with 0.60 in 3D.

4.2.1 Loss Rates

We now discuss the experimental feasibility of 2D condensates with $1/r$ interaction against losses. The main sources of depletion mechanism in a gravitylike interacting gas, in the TF-G and G regions, are losses due to $1/r^3$ oscillating interfering terms and those due to incoherent phonon scattering, namely Rayleigh scattering. The conditions necessary to observe the transition from external trapping to self-binding have been analyzed by O'Dell *et al.* [12] and Giovanazzi *et al.* [80] in the case of 3D condensates. They have shown that the Rayleigh scattering rate is reduced by a factor $(qR_{\rm rms})^2$ for sample sizes smaller than laser wavelength [12, 80]. Here q is the wave vector associated with the laser wavelength (i.e., $q = 2\pi/\lambda_L$) and $R_{\rm rms}$ is the root-mean-square of the condensate size proportional to the variational width parameter. Our numerical calculations for the TF-G region give $R_{\rm rms} \sim 0.46\,\lambda_L$ for the values $a \sim$ 3 nm, $a_* \sim$ 10 cm, and $\lambda_L = 10.6$ μm, which means that this region is experimentally accessible.

We calculate the temporal characteristics in relation to Rayleigh scattering rate by adopting the approach by Giovanazzi *et al.* [80] to a 2D condensate. In the TF-G and G regimes, characteristic time scale for the dynamics of the system can be estimated from the plasma frequency, which has the form

$$\omega_p^2 = \frac{4\pi^2 u \rho_{peak}}{m\lambda_L}\,, \tag{4.19}$$

in 2D [97], where ρ_{peak} is the peak density and λ_L is the laser wavelength. The Rayleigh scattering rate can be expressed as [80]

$$\Gamma_{Ray} = \frac{20\pi}{11}\frac{u}{\hbar\lambda_L}\,. \tag{4.20}$$

Using Equation 4.20 and recoil energy $E_R = \hbar^2 q^2/2m$, one can write the plasma frequency ω_p as

$$\omega_p = 0.72\frac{\Gamma_{Ray}^{3/2} N^{3/2}}{(E_R/\hbar)^{1/2}}\frac{1}{1+\tilde{s}}\,. \tag{4.21}$$

For a 2D condensate $a_z \gg a$, and the last quotient in the above expression goes to unity since $\tilde{s} \to 0$. Thus, for the parameters given in the Ref. [80], namely,

$N = 40$ atoms, $\Gamma_{Ray} = 1.58 \times 10^4\,\mathrm{s}^{-1}$ and recoil energy $E_R/\hbar = 1.57 \times 10^5\,\mathrm{s}^{-1}$, we find $\omega_p \approx 57\Gamma_{Ray}$ which is about three times the value in the 3D case [97]. This estimation shows that even for a small number of atoms the proposed laser characteristics and two-dimensional nature of the condensate allow for several oscillations of the self-bound gas within the Rayleigh lifetime.

One may also compare the monopole and quadrupole mode frequencies in the TF-G regime to the Rayleigh scattering rate. Recalling, for instance, $\omega_Q = 1.5462\omega_g S^{-3/2}$, the ratio of the TF-G quadrupole mode to the Γ_{Ray} is

$$\frac{\omega_Q}{\Gamma_{Ray}} = 0.94\frac{\hbar\Gamma_{Ray}N^2S^{-3/2}}{E_R}\,. \tag{4.22}$$

For the parameters given above, we find that $\omega_Q/\Gamma_{Ray} < 53$ for $S < 2$ and $\omega_Q/\Gamma_{Ray} < 1$ for $S > 28$. Our estimation again shows that excitations can be observed experimentally within the Rayleigh lifetime.

4.3 Vortex States

Vortices in Bose-Einstein condensed systems are important as they experimentally reveal the macroscopic phase coherence properties. To study the vortex states we again use the time-dependent variational analysis and choose the variational wavefunction for the self-bound gas as

$$\psi(\mathbf{r},t) = \sqrt{\frac{N}{\pi q!\alpha^{2q+2}}}r^q \exp\left(-\frac{r^2}{2}[1/\alpha(t)^2 + i\beta(t)]\right)\exp\left(iq\phi\right), \tag{4.23}$$

which vanishes as $r \to 0$, and q is the vortex quantum number. By using the same Lagrangian density in Equation (4.9), we obtain the Lagrangian

$$L = \frac{SN^2u^2}{g}\left[(q+1)\alpha^2\dot{\beta} - (q+1)\left(\frac{1}{\alpha^2} + \alpha^2\beta^2\right) - \frac{g_q}{\pi}\frac{S}{\alpha^2} + \sqrt{\frac{\pi}{2}}\frac{c_q}{\alpha}\right], \tag{4.24}$$

where $g_q = (2q)!/2^{2q}(q!)^2$, $c_1 = 7/16$, and $c_2 = 321/1024$. Then, one can find the energy of the vortex state as

$$E_q = \frac{SN^2u^2}{g}\left[(q+1)\frac{1}{\alpha^2} + \frac{g_q}{\pi}\frac{S}{\alpha^2} - \sqrt{\frac{\pi}{2}}\frac{c_q}{\alpha}\right]. \tag{4.25}$$

Equilibrium point is found by minimizing the energy

$$\sigma_q = \sqrt{\frac{2}{\pi}} \left[\frac{2(q+1) + \frac{2}{\pi} g_q S}{c_q} \right]. \tag{4.26}$$

The balance between the kinetic energy and the interaction energy terms fixes the structure of the vortex core. The coherence length ξ is a measure of the superfluid characteristics of the system which is obtained by equating these energies:

$$\frac{\hbar^2}{2m\xi} = \frac{gN}{2R^2} - \frac{uN}{\xi}, \tag{4.27}$$

where $R = g\sqrt{F}/2uS$ is the radius of the condensed state and $F = -\left[\frac{1}{\sigma^2} + \frac{S}{\pi\sigma^2} - \sqrt{\frac{\pi}{2}}\frac{1}{\sigma}\right]$, in which σ is the equilibrium width without vortices. Thus, the coherence length is

$$\frac{\xi}{R} = \frac{\sqrt{F} + \sqrt{F + 2S}}{2S}. \tag{4.28}$$

The coherence length as a function of the scattering parameter S is shown in Figure 4.3. For small values of the scattering parameter, ξ/R is seen to be very large which implies that superfluidity is destroyed. As the scattering length increases, the coherence length is getting much smaller, i.e. the system keeps displaying superfluidity.

The critical angular frequency to create a vortex is found by using the energies of the vortex and vortex-free states as

$$\Omega_q = \frac{\omega_g}{2} \left[\frac{2}{\sigma_q^2} - \frac{1}{\sigma^2} + \frac{S}{2\pi} \left(\frac{1}{2\sigma_q^2} - \frac{1}{2\sigma^2} \right) - \sqrt{\frac{\pi}{2}} \left(\frac{7}{16\sigma_q} - \frac{1}{\sigma} \right) \right]. \tag{4.29}$$

In Figure 4.4, we present the behavior of the critical angular frequency for one vortex. From the inset one can see that Ω_1 increases for negative S, i.e., for attractive interaction it is harder to create a vortex, and it decreases as the scattering parameter increases.

The frequency of the monopole mode for the vortex state is obtained as

$$\omega_q^2 = \left[\frac{3}{\sigma_q^4} + \frac{3 g_q S}{\pi(q+1)\sigma_q^4} - \sqrt{\frac{\pi}{2}} \frac{c_q}{(q+1)\sigma_q^3} \right], \tag{4.30}$$

where σ_q is defined in Equation (4.26). In the presence of vortices, the system collapses at $S = -(q+1)\pi/g_q$.

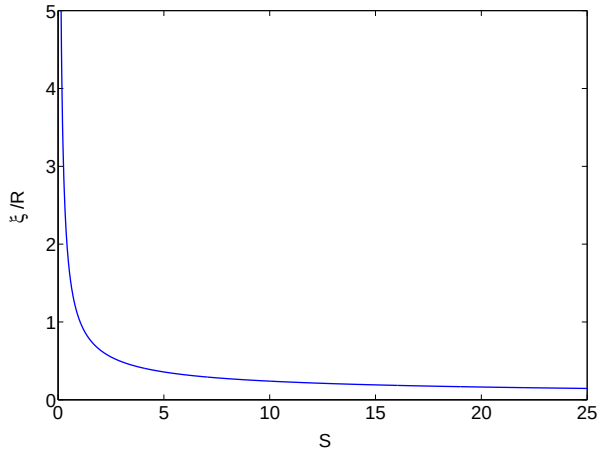

Figure 4.3: Coherence length as a function of the dimensionless scattering parameter S.

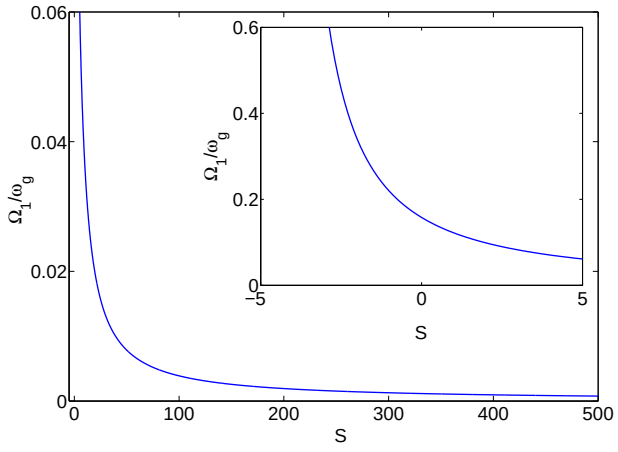

Figure 4.4: Critical angular frequency for $q = 1$ as a function of the dimensionless scattering parameter S. Inset is a zoom plot for negative S values.

TF-G regime: When the s-wave scattering length is very large, the kinetic energy contribution can be neglected. Using Equation (4.28), the superfluid coherence length is obtained as $\xi/R = 0.7071S^{-1/2}$ where $F = 1.23S^{-1}$. As S increases, the coherence length gets smaller compared to the size of the condensate, i.e. superfluid properties are observed in the TF-G regime. The critical angular frequencies needed to create vortices are $\Omega_1 = 0.3808\omega_g S^{-1}$ and $\Omega_2 = 0.2277\omega_g S^{-1}$ for $q = 1$ and $q = 2$, respectively. Unlike in the 3D case, these two frequencies are larger than the chemical potentials μ_1 and μ_2, thus the condensate state with a vortex is unbounded in this regime.

G regime: In this regime s-wave interaction energy is very small, so it is neglected. The radius of the condensate is $R_g = g\sqrt{F}/2uS$ and the superfluid coherence length is $\xi = 0.798R_g$, close to the radius of the condensate, which means that superfluidity disappears. This ratio is larger in the 3D system [81]. The critical angular frequencies are $\Omega_1 = 0.1776\omega_g$ and $\Omega_2 = 0.095\omega_g$ for q=1 and q=2, respectively, and Ω_2 is much less than Ω_1. The chemical potentials in the rotating frame are $|\mu_1|/\hbar = 0.0188\omega_g$ and $|\mu_2|/\hbar = 0.0065\omega_g$. In this regime, only one monopole mode is stable: $\omega_1 = 0.0188\omega_g$. For $q = 2$, monopole mode frequency $\omega_2 = 0.0096\omega_g > -\mu/\hbar$, which means that this oscillation is unstable and particles can escape from the condensate.

Chapter 5

Harmonically Trapped D-dimensional Ideal Gas Obeying Generalized Exclusion Statistics

Particle statistics drastically affect thermodynamic properties of quantum many-body systems. Fundamental particles obey either Bose-Einstein or Fermi-Dirac statistics and these bosonic or fermionic nature successfully describe many physical phenomena.

In 1991, Haldane introduced the so called fractional statistics or generalized exclusion statistics (GES) after observation of quasi-particles that have intermediate statistics between bosons and fermions in one and two dimensional systems [98]. Haldane formulated the generalized Pauli exclusion principle. He defined the GES through the linear relation

$$\Delta d_i = -\sum_j g_{ij} \Delta N_j, \tag{5.1}$$

where Δd_i is the change of the available single-particle states number, ΔN_j is the change of the particle numbers at fixed size and boundary conditions and i, j indicate different particle species. By adopting a state-counting definition, Wu proposed the occupation number distribution of particles which obey fractional statistics [99].

There has been a growing interest in GES since Haldane's formulation. It has been shown that the anyon gas in the lowest Landau level satisfies the GES [98–101]. Several researchers have studied the thermodynamic properties of the ideal g-on gas by using different methods [102–108]. Various systems have been also studied such as 1D and 2D Bose gas [109, 110], ideal and interacting quantum gases [111, 112]. Hansson *et al.* [110] established that a $2D$ Bose gas with a repulsive delta-function interaction obeys exclusion statistics and is equivalent to an ideal exclusion statistics gas by a direct counting of states. Different descriptions for the occupation number were proposed [113, 114]. Recently, Bhaduri *et al.* [115] calculated the chemical potential and the energy of the gas of neutral fermionic atoms by assuming the system to be an ideal gas which obeys Haldane-Wu statistics. They also presented the results for harmonically trapped gas. In a very recent paper , Potter *et al.* [116] explored the thermodynamics of the generalized Calogero-Sutherland model in $D \geq 1$ dimensions and also studied the effects of soft container walls. In two recent papers [117, 118], it is shown that $1D$ interacting anyons and bosons in the strong coupling regime are properly described by GES and the quasiparticle excitations of these two systems also obey GES. Batchelor *et al.* [101] showed that the distribution profiles of strongly interacting $1D$ anyon gas and Bose gas are equivalent to the most probable distribution profiles of ideal particles obeying fractional statistics.

In this chapter, we calculate the thermodynamic properties of the ideal gas within the generalized exclusion statistics (g-on gas) trapped with a harmonic potential in D dimensions [119]. Other than the above related works, we are also motivated by a recent proposal by Paredes *et al.* [120] to observe fractional statistics of anyons in a system of ultra-cold bosonic atoms in a rapidly rotating trap. Generally, harmonic potentials created by magneto-optical techniques, are used for trapping the ultra-cold Bose gases. We assume that the particles have the energy spectrum of the form $\varepsilon(p) = ap^s$ and neglect the spin degree of freedom. We calculated the specific heat of the ideal trapped g-on gas in several spatial dimensions and with different dispersion relations. It is important to establish the thermodynamic properties of ideal gas systems before tackling the interaction

effects.

5.1 Generalized Exclusion Statistics

The number of quantum states of N identical bosons or fermions occupying G states is

$$\begin{aligned} W_B &= \frac{(G+N-1)!}{N!(G-1)!}, \\ W_F &= \frac{G!}{N!(G-N)!}, \end{aligned} \tag{5.2}$$

respectively.

Wu [99] interpolated the number of quantum states for bosons and fermions and defined the statistical weight of N identical particles occupying a group of G states as

$$W = \prod_i \frac{[G_i + (N_i - 1)(1-g)]!}{N_i![G_i - gN_i - (1-g)]!}. \tag{5.3}$$

This weight corresponds to bosons when $g = 0$ and to fermions when $g = 1$. The parameter g characterizes the generalized Pauli exclusion principle since the occupation number for single-particle state has a maximum value of $1/g$.

To study quantum statistical mechanics of g-on gas, we start with a grand canonical ensemble at temperature T and with chemical potential μ. The grand canonical partition function is

$$Z = \sum_{\{N_i\}} W(\{N_i\}) \exp[-\beta \sum_i N_i(\varepsilon_i - \mu)]. \tag{5.4}$$

The summand in partition function has a very sharp peak around the set of most probable particle numbers $\{N_i\}$ for very large G_i and N_i. Thus, the most probable distribution is determined by

$$\frac{\partial}{\partial f_i} \ln Z = 0, \tag{5.5}$$

where $f_i = N_i/G_i$ is the average occupation number. Then, the average occupation number satisfies the relation

$$f_i \mathrm{e}^{(\varepsilon_\mathrm{i}-\mu)/\mathrm{kT}} = (1 - \mathrm{gf_i})^{\mathrm{g}}(1 + (1-\mathrm{g})\mathrm{f_i})^{1-\mathrm{g}} \tag{5.6}$$

Finally, the distribution function in generalized exclusion statistics is given as [99]

$$f(\varepsilon) = \frac{1}{w+g}, \tag{5.7}$$

where w obeys the relation

$$w^g(1+w)^{1-g} = \exp[\beta(\varepsilon-\mu)], \tag{5.8}$$

in which $\beta = 1/T$ (temperature is in units of Boltzmann constant) and μ is the chemical potential. One can see from the Equation 5.8 that, for $g = 0$ (1), the distribution function reduces to the bosonic (fermionic) form. One should note that $f \leq 1/g$, since $\mathrm{e}^{\beta(\varepsilon-\mu)}$ is always positive. The average occupation number at zero temperature obeys a step distribution like fermions

$$f(\varepsilon) = \begin{cases} \frac{1}{g} & (\varepsilon-\mu) \leq 0, \\ 0 & (\varepsilon-\mu) \geq 0. \end{cases} \tag{5.9}$$

5.2 Density of States and Thermodynamic Quantities

In the semi-classical approach, the density of states (DOS) for the particles in a harmonic potential in the D-dimensional space is calculated as

$$D(\varepsilon) = \int \frac{d^D r\, d^D p}{(2\pi\hbar)^D}\, \delta\left[\varepsilon - \left(\varepsilon(p) + \frac{1}{2}m\omega^2 r^2\right)\right]. \tag{5.10}$$

Here it is assumed that the system is in the thermodynamic limit, i.e. the number of particles $N \to \infty$, the volume $V \to \infty$, such that the number density N/V is constant. Thus, possible corrections to the DOS when the number of particles are finite are not included. Furthermore, because we have an inhomogeneous system due to the harmonic trap, the volume has to be understood as $V = \omega^{-D}$ in a D-dimensional space [121].

Using the properties of the delta-function, one can perform the r-integral,

$$D(\varepsilon) = \frac{S_D^2\, 2^{\frac{D-2}{2}}\, \varepsilon^{\frac{D-2}{2}}}{(2\pi m^{1/2})^D(\hbar\omega)^D} \int_0^{(\varepsilon/a)^{1/s}} dp\, p^{D-1}\left(1 - \frac{ap^s}{\varepsilon}\right), \tag{5.11}$$

where $S_D = \frac{2\pi^{D/2}}{\Gamma(D/2)}$ is the D-dimensional surface area. Finally, the DOS is

$$D(\varepsilon) = \frac{S_D^2\, 2^{\frac{D-2}{2}}}{(2\pi m^{1/2})^D s a^{D/s}} \frac{\Gamma(D/s)\Gamma(D/2)}{\Gamma(\frac{D}{s}+\frac{D}{2})} \frac{\varepsilon^{\frac{D}{s}+\frac{D-2}{2}}}{(\hbar\omega)^D}\,. \tag{5.12}$$

For a given density of states $D(\varepsilon)$ we have

$$\begin{aligned} N &= \int_0^\infty f(\varepsilon) D(\varepsilon) d\varepsilon, \\ E &= \int_0^\infty f(\varepsilon)\varepsilon D(\varepsilon) d\varepsilon. \end{aligned} \tag{5.13}$$

for the number of particles N in the system and the total energy E, respectively.

At $T = 0$, the Fermi energy is found as

$$\varepsilon_F = \left[\frac{Ng}{\gamma}\left(\frac{D}{s}+\frac{D}{2}\right)\right]^{1/\left(\frac{D}{s}+\frac{D}{2}\right)}, \tag{5.14}$$

where $\gamma = \frac{S_D^2 2^{\frac{D-2}{2}}}{(2\pi m^{1/2})^D s a^{D/s}} \frac{\Gamma(D/s)\Gamma(D/2)}{\Gamma(\frac{D}{s}+\frac{D}{2})} \frac{1}{(\hbar\omega)^D}$. The energy per particle is

$$\frac{E}{N} = \frac{\left(\frac{D}{s}+\frac{D}{2}\right)}{\left(\frac{D}{s}+\frac{D+2}{2}\right)}\varepsilon_F. \tag{5.15}$$

At finite temperature energy per particle can be calculated similarly. Converting the integration variable ε to w, for N and E we get

$$1 = \left(\frac{D}{s}+\frac{D}{2}\right)\left(\frac{T}{\epsilon_F}\right)^{\left(\frac{D}{s}+\frac{D}{2}\right)} \int_{w_0}^\infty \frac{dw}{w(1+w)} \left\{\ln\left[\left(\frac{w}{w_0}\right)^g \left(\frac{1+w}{1+w_0}\right)^{1-g}\right]\right\}^{\left(\frac{D}{s}+\frac{D-2}{2}\right)}, \tag{5.16}$$

and

$$\frac{E}{N\epsilon_F} = \left(\frac{D}{s}+\frac{D}{2}\right)\left(\frac{T}{\epsilon_F}\right)^{\left(\frac{D}{s}+\frac{D+2}{2}\right)} \int_{w_0}^\infty \frac{dw}{w(1+w)} \left\{\ln\left[\left(\frac{w}{w_0}\right)^g \left(\frac{1+w}{1+w_0}\right)^{1-g}\right]\right\}^{\left(\frac{D}{s}+\frac{D}{2}\right)}, \tag{5.17}$$

where w_0 is the value of w at $\varepsilon = 0$, $w_0^g(1+w_0)^{1-g} = \exp(-\beta\mu)$ and ϵ_F is the Fermi energy at $g = 1$. One can calculate the specific heat readily using $C_v = \frac{\partial E}{\partial T}$.

$$C_v = \int d\varepsilon D(\varepsilon)\varepsilon \frac{\partial}{\partial T}\frac{1}{w+g}, \tag{5.18}$$

and after some algebra specific heat per particle is given as

$$C_v = \int d\varepsilon D(\varepsilon)\varepsilon \left[\frac{\varepsilon-\mu}{T^2} + \frac{1}{T}\frac{\partial\mu}{\partial T}\right]\frac{w(1+w)}{(w+g)^3}. \tag{5.19}$$

We can find the $\frac{\partial\mu}{\partial T}$ using Equation 5.16 and the Leibniz integral rule as

$$\begin{aligned}\frac{\partial\mu}{\partial T} = &- \ln[w_0^g(1+w_0)^{1-g}] \\ &- \frac{\left(\frac{D}{s}+\frac{D}{2}\right)}{\left(\frac{D}{s}+\frac{D-2}{2}\right)}\frac{\int_{w_0}^{\infty}\frac{dw}{w(1+w)}\left\{\ln\left[\left(\frac{w}{w_0}\right)^g\left(\frac{1+w}{1+w_0}\right)^{1-g}\right]\right\}^{\left(\frac{D}{s}+\frac{D-2}{2}\right)}}{\int_{w_0}^{\infty}\frac{dw}{w(1+w)}\left\{\ln\left[\left(\frac{w}{w_0}\right)^g\left(\frac{1+w}{1+w_0}\right)^{1-g}\right]\right\}^{\left(\frac{D}{s}+\frac{D-4}{2}\right)}}.\end{aligned} \tag{5.20}$$

Then the specific heat can be written as

$$\begin{aligned}\frac{C_v}{N} = &\left(\frac{D}{s}+\frac{D}{2}\right)\left(\frac{T}{\epsilon_F}\right)^{\left(\frac{D}{s}+\frac{D}{2}\right)}\int_{w_0}^{\infty}\frac{dw}{(w+g)^2}\left\{\ln\left[\left(\frac{w}{w_0}\right)^g\left(\frac{1+w}{1+w_0}\right)^{1-g}\right]\right\}^{\left(\frac{D}{s}+\frac{D}{2}\right)} \\ &\times \left\{\ln\left[\left(\frac{w}{w_0}\right)^g\left(\frac{1+w}{1+w_0}\right)^{1-g}\right]\right. \\ &- \left.\frac{\left(\frac{D}{s}+\frac{D}{2}\right)\int_{w_0}^{\infty}\frac{dw}{w(1+w)}\left\{\ln\left[\left(\frac{w}{w_0}\right)^g\left(\frac{1+w}{1+w_0}\right)^{1-g}\right]\right\}^{\left(\frac{D}{s}+\frac{D-2}{2}\right)}}{\left(\frac{D}{s}+\frac{D-2}{2}\right)\int_{w_0}^{\infty}\frac{dw}{w(1+w)}\left\{\ln\left[\left(\frac{w}{w_0}\right)^g\left(\frac{1+w}{1+w_0}\right)^{1-g}\right]\right\}^{\left(\frac{D}{s}+\frac{D-4}{2}\right)}}\right\}.\end{aligned} \tag{5.21}$$

To find the general relation between the pressure and the total energy we consider the thermodynamic potential Ω,

$$\Omega = -PV = -T\ln Z \tag{5.22}$$

where the grand canonical partition function is given in Equation 5.4.

In terms of the distribution in Equation 5.7 the thermodynamic potential is given by

$$\Omega = -PV = -T\sum_i G_i \ln\frac{1+(1-g)f_i}{1-gf_i} = -T\sum_i G_i \ln\left[1+\frac{1}{w}\right] \tag{5.23}$$

In the thermodynamic limit a sum can be replaced by an integration, then the pressure is

$$\frac{P}{T} = \gamma \int_0^\infty d\varepsilon \varepsilon^{\frac{D}{s}+\frac{D}{2}} \ln\left[1+\frac{1}{w}\right]. \tag{5.24}$$

Integrating by parts we obtain

$$\begin{aligned} \frac{P}{T} &= \frac{\beta}{\left(\frac{D}{s}+\frac{D}{2}\right)} \int_0^\infty f(\varepsilon)\varepsilon D(\varepsilon) d\varepsilon \qquad (5.25) \\ PV &= \frac{E}{\left(\frac{D}{s}+\frac{D}{2}\right)}. \end{aligned}$$

This is the so-called Bernouilli equation for a harmonically trapped ideal gas obeying generalized exclusion statistics. In the above derivation, although we have used the thermodynamic variables pressure P and volume V in the definition of the grand potential, their meaning for trapped systems deserves special attention as we have already remarked. As discussed by Romero-Rochin [121] recently, the volume can be identified as $V = \omega^{-D}$ in D-dimensional space and its conjugate variable harmonic pressure is $P = -(\partial\Omega/\partial V)_{T,\mu,}$.

Finally, the entropy of the system can be found using the relation $S = \frac{E}{T} + \ln Z - \frac{N\mu}{T}$. Then the entropy is obtained as

$$S = \frac{E}{T}\left[1+\frac{1}{\left(\frac{D}{s}+\frac{D}{2}\right)}\right] - \frac{N\mu}{T}. \tag{5.26}$$

The above result is slightly different from the entropy found by Yang [108] since they did the calculations for the uniform gas.

5.3 Results and Discussion

Based on the theoretical formulation of the thermodynamic quantities of an ideal g-on gas in D-dimensions, we now present some illustrative examples.

For a 3D space and when $s = 2$, the total energy per particle as a function of temperature is shown in Figure 5.1. At low temperatures, the energy increases with g and at high temperature all curves have the same slope. The specific heat as a function of temperature is shown in Figure 5.2. The specific heat

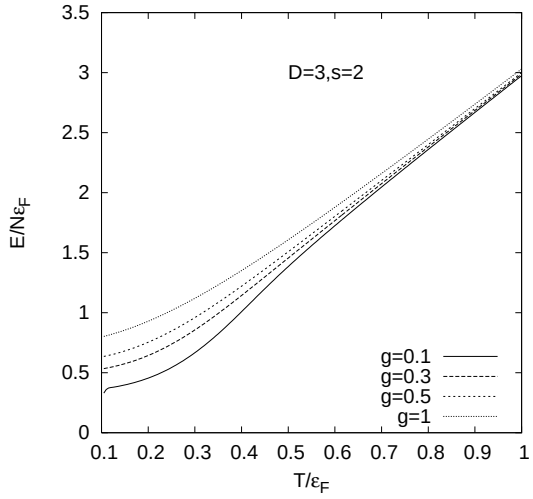

Figure 5.1: Energy per particle as a function of temperature in 3D for various values of the statistical parameter g.

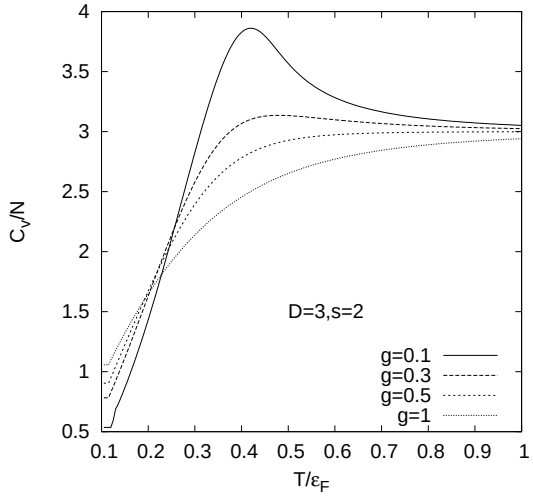

Figure 5.2: Specific heat per particle as a function of temperature in 3D for various values of the statistical parameter g.

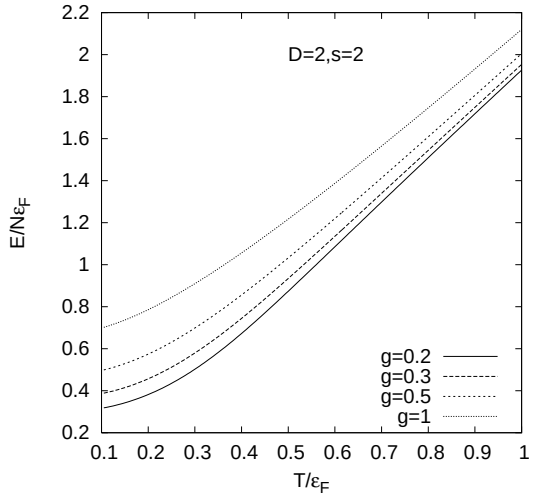

Figure 5.3: Energy per particle as a function of temperature in 2D for various values of the statistical parameter g.

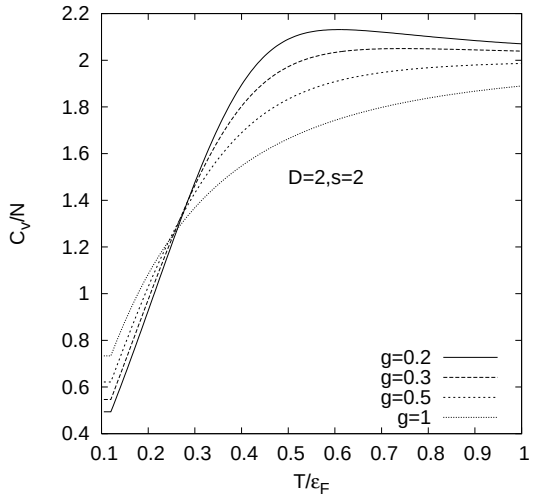

Figure 5.4: Specific heat per particle as a function of temperature in 2D for various values of the statistical parameter g.

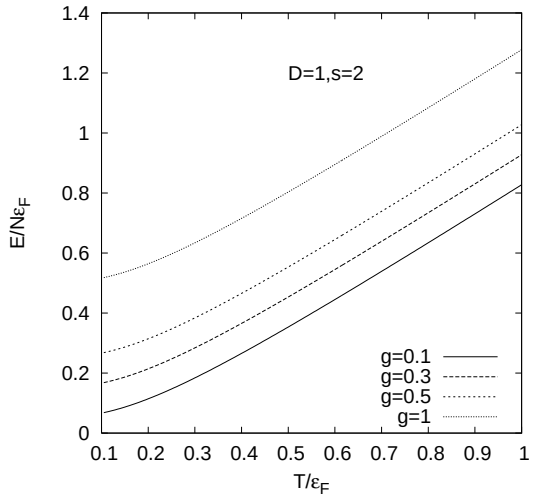

Figure 5.5: Energy per particle as a function of temperature in 1D for various values of the statistical parameter g.

increases with statistical parameter g at low temperatures and decreases at high temperatures reaching eventually the classical value in the high temperature regime. One can also see that it starts to exhibit bosonic behavior as g approaches 0. The energy and the specific heat for a 2D system are similar to 3D ones as shown in Figures 5.3 and 5.4, respectively.

Figures 5.5 and 5.6 show the interesting case where the density of states is constant ($D = 1$, $s = 2$) of the energy and specific heat, respectively. We observe in Fig. 5 that the energy curves for various g values differ by a temperature independent constant and in Figure 5.6 that the specific heat does not depend on the statistical parameter g. Similarly, the entropy S also becomes independent of g. It is known that for a constant density of states differences between bosons and fermions disappear, and as far as the thermodynamics is concerned the systems are said to be equivalent. For an ideal uniform system the constant density of states and consequently the same specific heat for bosons and fermions takes place in 2D for quadratic dispersion [106, 122].

Finally, for a system which has energy dispersion $\varepsilon \sim p$ in 1D, the energy

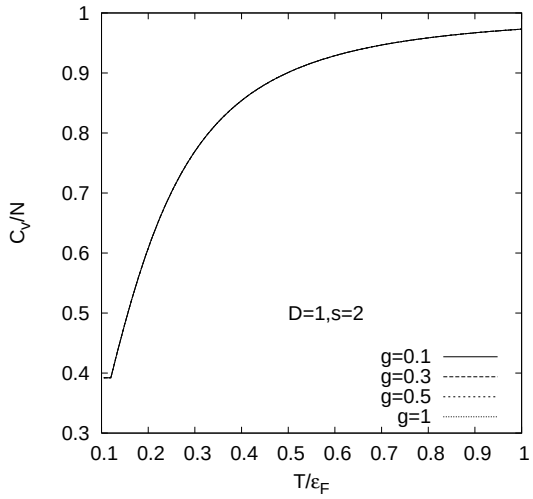

Figure 5.6: Specific heat per particle as a function of temperature in 1D. In this case, specific heat does not depend on the statistical parameter g.

and specific heat are shown in Figures 5.7 and 5.8, respectively. Interestingly, we have the same total energy relation with the uniform system that has energy dispersion $\varepsilon \sim p^2$ in 3D [106]. There is a critical temperature at which the specific heat does not depend on g. It means that there is no difference between bosons and fermions at this specific temperature. Below this temperature the entropy increases with g, but it decreases above this critical temperature. Similar behavior can be observed for other spatial dimensions and dispersion relations.

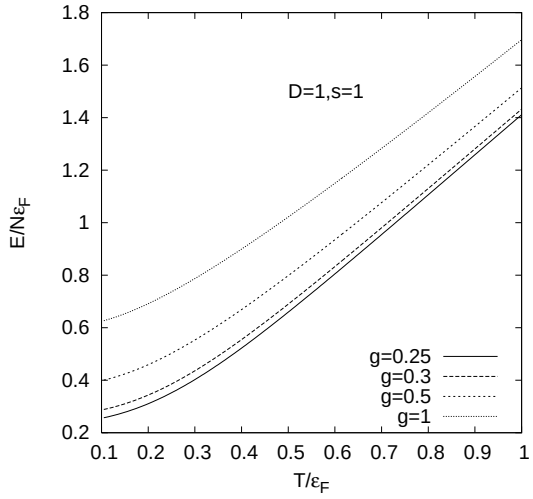

Figure 5.7: Energy per particle as a function of temperature in 1D and linear dispersion relation $\varepsilon \sim p$.

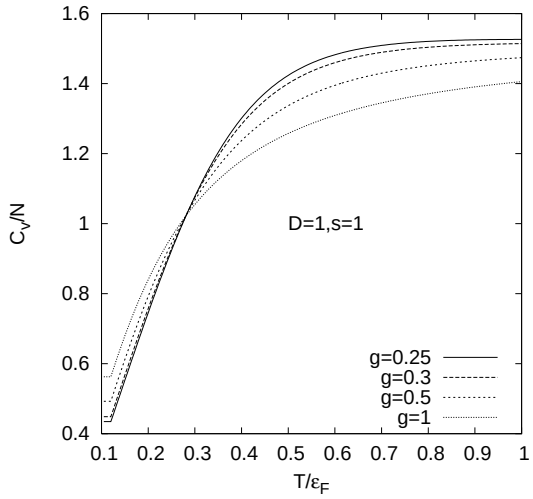

Figure 5.8: Specific heat per particle as a function of temperature in 1D and linear dispersion relation $\varepsilon \sim p$.

Chapter 6

Conclusions

The way to simulate quantum systems and to realize many-body models has been opened by the progress in the experimental manipulation of dilute ultra-cold atomic gases. These systems offer very interesting and novel research possibilities both theoretically and experimentally. In this thesis, we study selected topics on ultra-cold atomic gas systems theoretically. We investigate the ground-state properties, collective phenomena, behavior in optical lattices, and thermodynamics of these ultra-cold atomic systems. The results we obtained can be summarized as follows.

In Chapter 2, we have calculated the dependence of the size of a Bose condensed ionic cloud on the electron density for the system of degenerate ultra-cold plasma, using Thomas-Fermi screening picture. This result may be used as a starting point for more accurate calculations of the plasma density, and is directly relevant for the design of traps that can hold degenerate ultra-cold plasma. Our calculations show that to obtain stable ultra-cold plasma of similar sizes to current experiments, trapping frequencies must of the order of tens of KHz. We have also calculated the size of the cloud for the same system, but for the case that density of electrons is assumed as a dynamical variable. Instead of using variational method we calculated the electron and ion densities by means of Thomas-Fermi model. Although the variational model is not so accurate, the result obtained from this model is in good agreement with the latter result.

Complete screening of plasma is obvious in this system since ion and electron densities are completely the same. For 10^4 ions and 10^4 electrons cloud size is found as $14\,\mu m$ when the order of the trapping frequency is 10 KHz.

In Chapter 3, we have studied the localization of a single fermionic particle in a cubic optical lattice containing a Mott insulator of bosons. The impurity particle has two types of behavior; it may either move freely throughout the lattice or may choose to localize at a certain lattice site by attracting extra bosons or holes. In the limit of a perfect Mott insulator (MI), we have calculated the boundary between these two phases as well as the number of extra bosons (holes) forming the bound state exactly. Our result for the phase diagram is given in Figure 3.2, and we believe that this phase diagram can be checked experimentally. In recent experiments boson-fermion mixtures were created in the parameter regimes that we consider in this chapter [65, 66]. After the ideal case, we considered two effects which may play a role in the experiments. The first one we consider is the possibility of tunnelling anisotropy that experiments usually have. We have generalized the exact results to this case and find that it becomes easier to localize the impurity when the system becomes more two dimensional, as expected. Finally, we considered the effect of higher bands of the impurity particle. It is argued that this effect can be taken into account by modifying the hopping strengths between the localization site and its neighbors, and we obtained the phase diagram. We believe that our exact results about impurity localization on a Mott insulator background provide a starting point for the investigation of the complex phase diagram of mixtures in optical lattices.

In Chapter 4, we have studied a 2D condensate with attractive gravitylike $1/r$ interaction. We have shown that the laser-induced attractive $1/r$ interaction gives rise to a stable condensate in the 2D without a trap as it is in the 3D case. Unlike the 3D case, there is no collapse till $\tilde{s} = -1$. We have calculated the experimental quantities such as the release energy, the peak velocity and the condensate radius for ideal noninteracting (I), ordinary Thomas-Fermi (TF-O), Thomas-Fermi gravity (TF-G), and gravity (G) regions. We have also studied the dynamics of the system and calculated the monopole and quadrupole frequencies

and analyzed them within the TF-G and G regimes. These modes depend on the scattering length a in the TF-G regime unlike the ordinary TF regime. We have shown that the monopole mode exists not only for positive S values but also for negative values down to $S = -\pi$, in contrast to the situation in 3D [81] where the monopole mode exists for $S > 0$ only. Our estimate of the main loss mechanism, namely, the Rayleigh scattering, shows that these collective oscillations may be observed in 2D condensates for reasonable parameters. We have also investigated the vortex states and calculated the energy, the coherence length, the critical angular frequencies, and the monopole mode frequencies for $q = 1, 2$. The presence of vortices in the condensate extends the range of S in which the condensate is stable. As the scattering parameter increases, the system keeps displaying superfluidity since the coherence length is getting smaller. We have examined the TF-G and G regimes and have shown that in the TF-G regime the condensate state is unbounded. In the G regime, superfluidity disappears and only the monopole mode for the vortex state for $q = 1$ is stable. The results of our calculations should be useful in analyzing experiments performed on 2D condensates. Distinctive features of collective modes may help the identification of 2D nature of condensates in various regimes compared to the 3D case.

In Chapter 5, we have considered ideal gases trapped by a harmonic oscillator potential in D-dimensions and obeying the generalized exclusion statistics. Thermodynamic properties such as energy and specific heat as functions of temperature are calculated numerically for various spatial dimensions and single-particle energies. Illustrative examples are presented for various values of the statistical parameter g. As trapped systems of atomic gases are of growing interest in recent years, we expect our results will be useful for further studies.

Briefly, we have investigated the ground-state properties of a number of quantum gaseous systems at zero temperature in this thesis. First, the cloud size and electron and ion densities have been calculated for the system of trapped, degenerate ultra-cold plasma. Then, localization problem of a single-particle on a Mott insulator background has been investigated. Next, the ground-state properties, dynamics, and vortex states for 2D condensate with gravitylike

attraction have been studied and finally, thermodynamics of ideal gas obeying generalized exclusion statistics for several dimensions and dispersion relations has been analyzed.

Bibliography

[1] M. H. Anderson, J. R. Ensher, M. R. Matthews, C. E. Wieman, and E. A. Cornell, Science **269**, 199 (1995).

[2] K. B. Davis, M.-O. Mewes, M. R. Andrews, N. J. van Druten, D. S. Durfee, D. M. Kurn, and W. Ketterle, Phys. Rev. Lett. **75**, 3969 (1995).

[3] A. Einstein, Sitzungsberg k. Preuss, Akad. Wiss. Phys. Math. **K1**, 3 (1925).

[4] S. N. Bose, Z. Phys. **26**, 178 (1924).

[5] C. J. Pethick, and H. Smith, *Bose-Einstein Condensation in Dilute Gases*, (Cambridge University Press, Cambridge, 2002).

[6] L. Pitaevskii, and S. Stringari, *Bose-Einstein Condensation*, (Clarendon Press, Oxford, 2003).

[7] B. DeMarco, and D. D. Jin, Science **285**, 1703 (1999).

[8] P. Courteille, R. Freeland, D. Heinzen, F. von Abeelen, and B. Verhaar, Phys. Rev. Lett. **81**, 69 (1998).

[9] S. Inouye, M. Andrews, J. Strenger, H. J. Miesner, S. Stemper-Kurn, and W. Ketterle, Nature **392**, 151 (1998).

[10] M. Greiner, O. Mandel, T. Esslinger, T.W. Hansch, and I. Bloch, Nature **415**, 39 (2002).

[11] D. Jaksch, C. Bruder, J.I. Cirac, C.W. Gardiner, and P. Zoller, Phys. Rev. Lett. **81**, 3108 (1998).

[12] D. O'Dell, S. Giovanazzi, G. Kurizki, and V.M. Akulin, Phys. Rev. Lett. **84**, 5687 (2000).

[13] A. Griesmaier, J. Werner, S. Hensler, J. Stuhler, and T. Pfau, Phys. Rev. Lett. **94**, 160401 (2005).

[14] F. Dalfovo, S. Giorgini, L. P. Pitaevskii, and S. Stringari, Rev. Mod. Phys. **71**, 463 (1999).

[15] N. Bogoliubov, J. Phys. (Moscow) **11**, 23 (1947).

[16] E. P. Gross, Nuovo Cimento **20**, 454 (1961).

[17] L. P. Pitaevskii, Sov. Phys. JETP **13**, 451 (1961).

[18] T. C. Killian, S. Kulin, s. D. Bergeson, L. A. Orozco, C. Orzel, S. L. Rolston, Phys. Rev. Lett. **83**, 4776 (1999).

[19] C. E. Simien, Y. C. Chen, P. Gupta, S. Laha, Y. N. Martinez, P. G. Mickelson, S. B. Nagel, T. C. Killian, Phys. Rev. Lett. **92**, 143001 (2004).

[20] E. A. Cummings, J. E. Daily, D. S. Durfee, S. D. Bergeson, Phys. Rev. Lett. **95**, 235001 (2005).

[21] M. P. Robinson, B. L. Tolra, M. W. Noel, T. F. Gallagher, P. Pillet, Phys. Rev. Lett. **85**, 4466 (2000).

[22] T. F. Gallagher, P. Pillet, M. P. Robinson, B. Laburthe-Tolra, M. W. Noel, J. Opt. Soc. Am. B **20**, 1091 (2003).

[23] D. Ciampini, M. Anderlini, J. H. Müller, F. Fuso, O. Morsch, J. W. Thomsen, E. Arimondo, Phys. Rev. A **66**, 043409 (2002).

[24] T. C. Killian, Nature **429**, 815 (2004).

[25] T. Pohl, T. Pattard, J. M. Rost, Phys. Rev. A **70**, 033416 (2004).

[26] T. C. Killian, V. S. Ashoka, P. Gupta, S. Laha, S. B. Nagel, C. E. Simien, S. Kulin, S. L. Rolston, S. D. Bergeson, J. Phys. A **36**, 6077 (2003).

[27] S. D. Bergeson and R. L. Spencer, Phys. Rev. E **67**, 026414 (2003).

[28] A. N. Tkachev and S. I. Yakovlenko , JETP Lett. **73**, 66 (2001).

[29] S. Kulin, T. C. Killian, S. D. Bergeson, S. L. Rolston, Phys. Rev. Lett. **85**, 318 (2000).

[30] L. I. Minshikov and P. O. Fedichev , Z. Eksp. T. Fiziki.,**108**, 144 (1995).

[31] A. N. Tkachev and S. I. Yakovlenko, Quantum Electron. **31**, 1084 (2001).

[32] T. C. Killian, M. J. Lim, S. Kulin, R. Dumke, S. D. Bergeson, S. L. Rolston, Phys. Rev. Lett. **86**, 3759 (2001).

[33] T. Pohl, T. Pattard, J. M. Rost, Phys. Rev. A **68**, 010703 (2003).

[34] S. K. Dutta, D. Feldbaum, A. Walz-Flannigan, J. R. Guest, G. Raithel, Phys. Rev. Lett. **86**, 3993 (2001).

[35] T. C. Killian, Y. C. Chen, P. Gupta, S. Laha, Y. N. Martinez, P. G. Mickelson, S. B. Nagel, A. D. Saenz and C. E. Simien, J. Phys. B **38**, 351 (2005).

[36] A. P. Gavrilyuk, I. V. Krasnov, N. Y. Shaparev, JETP Lett. **76**, 423 (2002).

[37] S. A. Sekatskii and G. Dietler, Optics Commun. **210**, 251 (2002).

[38] D. M. Stamper-Kurn, M. R. Andrews, A. P. Chikkatur, S. Inouye, H.-J. Miesner, J. Stenger, and W. Ketterle, Phys. Rev. Lett. **80**, 2027 (1998).

[39] S. R. Granade, M. E. Gehm, K. M. O'Hara, and J. E. Thomas, Phys. Rev. Lett. **88**, 120405 (2002).

[40] J. -H. Choi, B. Knuffman, X. H. Zhang, A. P. Povilus, and G. Raithel, Phys. Rev. Lett. **100**, 175002 (2008).

[41] S. Sevinçli, M. Ö. Oktel, and B. Tanatar, Phys. Lett. A **350**, 129 (2006)

[42] C. Kittel, *Introduction to Solid State Physics* (Wiley, New York, 1996).

[43] S. Sevinçli, M. Ö. Oktel, and B. Tanatar, Concepts of Phys. **4**, 461 (2007)

[44] L. D. Landau, E. M. Lifshitz, *Quantum Mechanics*, (Pergamon, Oxford, 1994).

[45] T. C. Killian, T. Pattard, T. Pohl, J. M. Rost, Phys. Reports **449**, 77 (2007).

[46] Y. E. Kim and A. L. Zubarev , Phys. Rev. A **64**, 013603 (2001).

[47] Y. C. Chen, C. E. Simien, S. Laha, P. Gupta, Y. N. Martinez, P. G. Mickelson, S. B. Nagel, and T. C. Killian, Phys. Rev. Lett. **93**, 265003 (2004).

[48] B. Paredes, A. Widera, V. Murg, O. Mandel, S. Folling, I. Cirac, G. V. Shlyapnikov, T. W. Hasch, and I. Bloch, Nature **429**, 277 (2004).

[49] J. K. Chin, D. E. Miller, Y. Liu, C. Stan, W. Setiawan, C. Sanner, K. Xu, and W. Ketterle, Nature **443**, 961 (2006).

[50] T. Stoferle, H. Moritz, K. Gunter, M. Kohl, and T. Esslinger, Phys. Rev. Lett. **96**, 030401 (2006).

[51] M. Anderlini, P. J. Lee, B. L. Brown, J. Sebby-Strabley, W. D. Phillips, and J. V. Porto, Nature **448**, 452 (2007).

[52] K. D. Nelson, X. Li, and D. S. Weiss, Nature Phys. **3**, 556 (2007).

[53] E. Altman, E. Demler, and M. D. Lukin, Phys. Rev. A **70**, 013603 (2004).

[54] M. P. A. Fisher, P. B. Weichman, G. Grinstein, and D. S. Fisher , Phys. Rev. B **40**, 546 (1989).

[55] I. Bloch, J. Dalibard, and W. Zwerger, Rev. Mod. Phys. **80**, 885 (2008).

[56] J. Goldwin, S. B. Papp, B. DeMarco, and D. D. Jin, Phys. Rev. A **65**, 021402(R) (2002).

[57] H. Ott, E. de Mirandes, F. Ferlaino, G. Roati, G. Modugno, and M. Inguscio, Phys. Rev. Lett. **92**, 160601 (2004).

[58] K. Mølmer, Phys. Rev. Lett. **80**, 1804 (1998).

[59] H. Heiselberg, C. J. Pethick, H. Smith, and L. Viverit , Phys. Rev. Lett. **85**, 2418 (2000).

[60] A. Albus, F. Illuminati, and J. Eisert, Phys. Rev. A **68**, 023606 (2003).

[61] A. B. Kuklov and B. V. Svistunov, Phys. Rev. Lett. **90**, 100401 (2003).

[62] M. Lewenstein, L. Santos, M. A. Baranov, and H. Fehrmann, Phys. Rev. Lett. **92**, 050401 (2004).

[63] U. Gavish and Y. Castin, Phys. Rev. Lett. **95**, 020401 (2005).

[64] K. Sacha and E. Timmermans, Phys. Rev. A **73**, 063604 (2006).

[65] K. Gunter, T. Stoferle, H. Moritz, M. Kohl, and T. Esslinger, Phys. Rev. Lett. **96**, 180402 (2006).

[66] S. Ospelkaus, C. Ospelkaus, O. Wille, M. Succo, P. Ernst, K. Sengstock, and K. Bongs, Phys. Rev. Lett. **96**, 180403 (2006).

[67] S. Sevinçli, R. O. Umucalılar, M. Ö. Oktel, arXiv:0709:4335 (2007).

[68] R. T. Delves and G. S. Joyce, J. Phys. A: Math. Gen. **34**, L59 (2001), and references therein.

[69] G. S. Joyce, J. Phys. A: Math. Gen. **5**, L65 (1972).

[70] M. W. Zwierlein, Z. Hadzibabic, S. Gupta, and W. Ketterle, Phys. Rev. Lett. **91**, 250404 (2003).

[71] C. Chin, M. Bartenstein, A. Altmeyer, S. Riedl, S. Jochim, J. H. Denschlag, and R. Grimm, Science **305**, 1128 (2004).

[72] G. S. Joyce, J. Phys. A: Math. Gen. **35**, 9811 (2002).

[73] H. Saito and M. Ueda, Phys. Rev. Lett. **90**, 040403 (2003).

[74] P. G. Kevrekidis, G. Theocharis, D. J. Frantzeskakis, and B. A. Malomed, Phys. Rev. Lett. **90**, 230401 (2003).

[75] G. D. Montesinos, V. M. Perez-Garcia, and H. Michinel, Phys. Rev. Lett. **92**, 133901 (2004).

[76] M. Matuszewski, E. Infeld, B. A. Malomed, and M. Trippenbach, Phys. Rev. Lett. **95**, 050403 (2005).

[77] J. Stuhler, A. Griesmaier, T. Koch, M. Fattori, T. Pfau, S. Giovanazzi, P. Pedri, and L. Santos, Phys. Rev. Lett. **95**, 150406 (2005).

[78] T. Thirunamachandran, Mol. Phys. **40**, 393 (1980).

[79] S. Giovanazzi, G. Kurizki, I. E. Mazets, and S. Stringari, Europhys. Lett. **56**, 1 (2001).

[80] S. Giovanazzi, D. O'Dell, and G. Kurizki, Phys. Rev. A **63**, 031603(R) (2001).

[81] T.K. Ghosh, Phys. Rev. A **65**, 053616 (2002).

[82] I. Papadopoulos, P. Wagner, G. Wunner, and J. Main, Phys. Rev. A **76**, 053604 (2007).

[83] K. Goral and L. Santos, Phys. Rev. A **66**, 023613 (2002).

[84] L. Santos, G. V. Shlyapnikov, and M. Lewenstein, Phys. Rev. Lett. **90**, 250403 (2003).

[85] S. Giovanazzi, L. Santos, and T. Pfau, Phys. Rev. A **75**, 015604 (2007).

[86] A. Posazhennikova, Rev. Mod. Phys. **78**, 1111 (2006).

[87] L. Pricoupenko, Phys. Rev. A **70**, 013601 (2004).

[88] L. D. Carr and C. W. Clark, Phys. Rev. Lett. **97**, 010403 (2006).

[89] U. R. Fischer, Phys. Rev. A **73**, 031602(R) (2006).

[90] A. Keleş, S. Sevinçli, and B. Tanatar, Phys. Rev. A **77**, 053604 (2008).

[91] M. D. Lee, S. A. Morgan, M. J. Davis, and K. Burnett, Phys. Rev. A **65**, 043617 (2002).

[92] L. Salasnich, A. Parola, and L. Reatto, Phys. Rev. A **65**, 043614 (2002).

[93] B. Tanatar, A. Minguzzi, P. Vignolo, and M. P. Tosi, Phys. Lett. A **302**, 131 (2002).

[94] L. Salasnich, Int. J. Mod. Phys. B **14**, 1 (2001).

[95] V. M. Perez-Garcia, H. Michinel, J. I. Cirac, M. Lewenstein, and P. Zoller, Phys. Rev. Lett. **77**, 5320 (1996).

[96] X.Z. Wang, Phys. Rev. D **64**, 124009 (2001).

[97] C. I. Um, W. H. Kahng, E. S. Yim, and T. F. George, Phys. Rev. B **41**, 259 (1990).

[98] F. D. M. Haldane, Phys. Rev. Lett. **67**, 937 (1991) .

[99] Y.-S. Wu, Phys. Rev. Lett. **73**, 922 (1994).

[100] A. K. Rajagopal, Phys. Rev. Lett. **74**, 1048 (1995).

[101] M. T. Batchelor, X.-W. Guan, and N. Oelkers, Phys. Rev. Lett. **96**, 210402 (2006).

[102] K. Iguchi, Phys. Rev. Lett. **78**, 3233 (1997).

[103] G. S. Joyce, S. Sarkar, J. Spalek, and K. Byczuk, Phys. Rev. B **53**, 990 (1996)

[104] S. B. Isakov and S. Ouvry, J. Phys. A: Math. Gen. **29**, 7401 (1996).

[105] S. B. Isakov, D. P. Arovas, J. Myrheim, and A. P. Polychronakos, Phys. Lett. A **212**, 299 (1996).

[106] T. Aoyama, Eur. Phys. J. B **20**, 123 (2001).

[107] G. Su and M. Suzuki, Eur. Phys. J. B **5**, 577 (1998).

[108] H. S. Yang, B. Lee, and C. Park, J. Kor. Phys. Soc. **30**, 14 (1996).

[109] R. K. Bhaduri, M. V. N. Murthy, and M. N. Tran, J. Phys. B: At. Mol. Op. Phys. **35**, 2817 (2002).

[110] T. H. Hansson, J. M. Leinaas, and S. Viefers, Phys. Rev. Lett. **86**, 2930 (2001).

[111] D. V. Anghel, J. Phys. A: Math. Gen. **35**, 7255 (2002).

[112] D.-V. Anghel, Phys. Rev. E **62**, 7658 (2000).

[113] W. Bao-Quan and W. Yu-Peng, Chin. Phys. Lett. **22**, 824 (2005).

[114] F. Büyükkılıç, H. Uncu, and D. Demirhan, Eur. Phys. J. B **35**, 111 (2003).

[115] R. K. Bhaduri, M. V. N. Murthy, and M. K. Srivastava, cond-mat/0606117.

[116] G. G. Potter, G. Muller, and M. Karbach, cond-mat/0610400.

[117] M. T. Batchelor, X. -W. Guan, and N. Oelkers, Phys. Rev. Lett. **96**, 210402 (2006).

[118] M. T. Batchelor, X. -W. Guan, Phys. Rev. B **74**, 195121 (2006).

[119] S. Sevinçli, and B. Tanatar,, Phys. Lett. A **371**, (2007) 389.

[120] B. Paredes, P. Fedichev, J. I. Cirac, and P. Zoller, Phys. Rev. Lett. **87**, 010402 (2001).

[121] V. Romero-Rochin, Phys. Rev. Lett. **94**, 130601 (2005).

[122] M. H. Lee, Phys. Rev. E **55**, 1518 (1997).